

# **Modelling of Molecule-Inside-Dipole Complexes: Through- vs. Around-Molecule Ion Transfer**

by

Stephen T.W. Kerr

A thesis submitted to the  
School of Graduate and Postdoctoral Studies in partial  
fulfillment of the requirements for the degree of

**Master of Science in Material Science**

University of Ontario Institute of Technology (Ontario Tech University)

Oshawa, Ontario, Canada

December 2023

© Stephen Kerr, 2023

## **THESIS EXAMINATION INFORMATION**

Submitted by: **Stephen Kerr**

### **Master of Science in Material Science**

Thesis title: Modeling of Molecule-Inside-Dipole Complexes: Through- vs. Around-Molecule Ion Transfer

An oral defence of this thesis took place on November/30/2023 in front of the following examining committee:

#### **Examining Committee:**

Chair of Examining Committee	Prof. Sean Bohun
Research Supervisor	Prof. Fedor Naumkin
Examining Committee Member	Prof. Anatoli Chkrebtsii
Thesis Examiner	Prof. Franco Gaspari

## ABSTRACT

This thesis explores computationally complexes of both polar (Tetraoxane/Pentaoxecane) and nonpolar (Cyclooctane) molecules with the Li-F ion pair, having potential applications in light-matter interactions, transmembrane ion-pair transport, and energy storage. Structures and stabilities, charge distributions, dipole moments, and infrared intensity spectra, are characterized for these systems. We find significant differences in the relative stabilities of complexes, with polar systems having increased stability and ion-attachment energies compared to non-polar systems. We have discovered energy barriers for  $\text{Li}^+$ 's ability to penetrate these three cyclic molecules. Interestingly, we report Tetraoxane's "flipped" complexation, trapped in-between Li-F with their dipole moments aligned additively, leading to a considerable dipole moment. Calculated infrared spectra show identifiable lines for insertion complexes and all conformations, promoting experimental detection. Overall, this research provides valuable insight into the design and application of such and similar molecular systems.

**Keywords:** chemistry; ab initio calculations; insertion complexes; dipole moment; ion transfer

## AUTHOR'S DECLARATION

I hereby declare that this thesis consists of original work of which I have authored. This is a true copy of the thesis, including any required final revisions, as accepted by my examiners.

I authorize the University of Ontario Institute of Technology (Ontario Tech University) to lend this thesis to other institutions or individuals for the purpose of scholarly research. I further authorize the University of Ontario Institute of Technology (Ontario Tech University) to reproduce this thesis by photocopying or by other means, in total or in part, at the request of other institutions or individuals for the purpose of scholarly research. I understand that my thesis will be made electronically available to the public.

A handwritten signature in black ink that reads "Stephen Kerr". The signature is written in a cursive style with a fluid, continuous flow of lines.

---

STEPHEN KERR

## **STATEMENT OF CONTRIBUTIONS**

I certify that I am the sole author of this thesis and that no part of this thesis has been published or submitted for publication. I have used standard referencing practices to acknowledge ideas, research techniques, or other materials that belong to others. Furthermore, I hereby certify that I am the sole source of the creative works and/or inventive knowledge described in this thesis.

## **ACKNOWLEDGEMENTS**

I am profoundly grateful to my thesis advisor, Fedor Naumkin. His patience and support gave me numerous opportunities to learn and grow. His belief in me gave me my first taste of research during my undergrad. He suggested I apply for grad school when I returned to finish my degree. His expertise and encouragement helped me to complete this research and write this thesis. Without his mentorship, I could not have undertaken this journey.

I would like to thank Anatoli Chkrebii, his late-night/weekend edits and comments on this thesis made all the difference. I would also like to thank all the teachers, teaching assistants, and tech staff at Ontario Tech who taught and helped me over the years.

I would also like to thank my friends and family for their love and support. Especially to my wife Selena and new son George, for their moral support. Without them, this adventure would not have been possible.

## TABLE OF CONTENTS

<b>Thesis Examination Information .....</b>	<b>ii</b>
<b>Abstract .....</b>	<b>iii</b>
<b>Authors Declaration .....</b>	<b>iv</b>
<b>Statement of Contributions.....</b>	<b>v</b>
<b>Acknowledgements .....</b>	<b>vi</b>
<b>Table of Contents .....</b>	<b>vii</b>
<b>List of Tables .....</b>	<b>ix</b>
<b>List of Figures.....</b>	<b>x</b>
<b>List of Abbreviations and Symbols .....</b>	<b>xii</b>
<b>Chapter 1 Introduction .....</b>	<b>1</b>
1.1 Application .....	1
1.1.1 Dipole moment .....	1
1.1.2 Ion-pair trapping .....	2
1.1.3 Design of ring-shaped molecule and potential ion-pair traps .....	3
1.1.4 Lithium penetrating .....	
4	
1.1.5 Ion-pair filtration .....	5
1.1.6 Analogous systems .....	5
1.1.6.1 Polar systems .....	5
1.1.6.2 Nonpolar systems .....	7
1.1.7 Infrared spectroscopy (IR) .....	8
1.2 Thesis Objectives .....	8
<b>Chapter 2 Body of the thesis .....</b>	<b>9</b>
2.0 Methods.....	9
2.1 Computational Chemistry .....	9
1.1.1 Schrödinger equation .....	10
1.1.2 Hamiltonian operator .....	11
1.1.3 Born-Oppenheimer Approximation .....	12
1.1.4 Hartree-Fock Self-Consistent Field Method .....	13
1.1.5 Møller Plesset Perturbation Theory .....	14
2.2 Methods .....	18
2.3 Results .....	20
2.4 Discussion .....	22
2.4.1 Tetraoxane .....	22
2.4.2 Pentaoxecane .....	33
2.4.3 Cyclooctane .....	41
2.4.4 Charges .....	50
<b>Chapter 3 Conclusions .....</b>	<b>52</b>
<b>Chapter 4 Future work .....</b>	<b>54</b>

4.0 Expansion of work.....	54
4.1 Self-assembly .....	54
4.2 2D network structure .....	55
4.3 Transmembrane ion-pair transport .....	56
<b>Bibliography .....</b>	<b>58</b>

## **LIST OF TABLES**

### **CHAPTER 2**

Table 2.1: Equilibrium parameters of Li-F (In brackets are experimental values <sup>1</sup> )....	18
Table 2.2: Energies, internal distances, and dipole moments. *For Tetraoxane (Flipped) systems Li-H and F-O distances are listed.....	20
Table 2.3: Ring gap area.....	21
Table 2.4: Charges from Electrostatic Potentials using a Grid-based method.....	21

## LIST OF FIGURES

### CHAPTER 1

Figure 1.0: Energy Density of Tetraoxane ..... 2

Figure 1.1: Dipole inside Dipole ..... 4

### CHAPTER 2

Figure 2.1.1: Comparison of Experimental and Calculated IR-Spectra for Cyclooctane  
(experimental top / Calculated Below)..... 19

Figure 2.4.1: Tetraoxane front view (left), and side view (right) ..... 22

Figure 2.4.2: Li-Tetraoxane-F complex ..... 22

Scheme 2.4.1: Dipoles components of Li-Tetraoxane-F complex Li-F (Left), Tetraoxane  
(middle), Li-Tetraoxane-F (Right) ..... 23

Figure 2.4.3: Tetraoxane-(Li<sup>+</sup>) ..... 23

Figure 2.4.4: (F<sup>-</sup>)-Tetraoxane ..... 24

Figure 2.4.5: Tetraoxane-F-Li. (F point) ..... 24

Figure 2.4.6: Tetraoxane Complex Energy Diagram ..... 25

Figure 2.4.7: Tetraoxane Li<sup>+</sup> Penetrating Energy Barriers ..... 26

Figure 2.4.8: F-Tetraoxane-Li. (Flipped) ..... 26

Figure 2.4.9: Tetraoxane -Li<sup>+</sup> (Flipped) ..... 27

Figure 2.4.10: Flipped Tetraoxane Complex Energy Diagram Energy Barriers..... 27

Figure 2.4.11: Li<sup>+</sup> Penetrating Flipped Tetraoxane ..... 28

Figure 2.4.12: F-Li-Tetraoxane. Li point ..... 29

Figure 2.4.13: Tetraoxane side attached ..... 29

Figure 2.4.14: Infrared Spectra of Li-Tetraoxane-F ..... 30

Figure 2.4.15: Infrared Spectra of Tetraoxane isolated ..... 30

Figure 2.4.16: Infrared Spectra of Li-F:Tetraoxane (side attached) ..... 31

Figure 2.4.17: Infrared Spectra of Tetraoxane combined. Red-side attached, blue-trapped,  
black-isolated ..... 32

Figure 2.4.18: Infrared Spectra of F-Li-Tetraoxane (Li point) .....	32
Figure 2.4.19: Infrared Spectra of Tetraoxane-F-Li (F point) .....	33
Figure 2.4.20: Pentaoxecane front view (left), side view (right) .....	34
Figure 2.4.21: Li-Pentaoxecane-F front view (left), side view (right) .....	34
Figure 2.4.22: Li <sup>+</sup> -Pentaoxecane .....	35
Figure 2.4.23: Pentaoxecane-F <sup>-</sup> .....	35
Figure 2.4.24: Pentaoxecane Complex Energy Diagram .....	36
Figure 2.4.25: Li <sup>+</sup> Penetrating Pentaoxecane Energy Barriers .....	37
Figure 2.4.26: F-Li-Pentaoxecane “Li point”.....	38
Figure 2.4.27: Pentaoxecane-Li-F side attached .....	38
Figure 2.4.28: Infrared Spectra of Pentaoxecane .....	39
Figure 2.4.29: Infrared Spectra of Pentaoxecane. Range 2700 cm <sup>-1</sup> -3200 cm <sup>-1</sup> .....	40
Figure 2.4.30: Infrared Spectra of Pentaoxecane. Range 750 cm <sup>-1</sup> -1500 cm <sup>-1</sup> .....	40
Figure 2.4.31: Infrared Spectra of Li-Pentaoxecane-F .....	41
Figure 2.4.32: Infrared Spectra of Li-Pentaoxecane-F. Range 2700 cm <sup>-1</sup> -3200 cm <sup>-1</sup> .....	41
Figure 2.4.33: Infrared Spectra of Li-Pentaoxecane-F. Range 750 cm <sup>-1</sup> -1500 cm <sup>-1</sup> .....	42
Figure 2.4.34: Cyclooctane front view ( <i>left</i> ), side view ( <i>right</i> ) .....	43
Figure 2.4.35: Li-Cyclooctane-F. Front View (Left), Side View (Right) .....	43
Figure 2.4.36: Cyclooctane:Li-F .....	44
Figure 2.4.37: Cyclooctane Complex Energy Diagram .....	44
.	
Figure 2.4.38: Li <sup>+</sup> Penetrating Cyclooctane Energy Barriers .....	45
Figure 2.4.39: Infrared Spectra of Cyclooctane .....	48
Figure 2.4.40: Infrared Spectra of Li-Cyclooctane-F .....	49
Figure 2.4.41: Infrared Spectra of Li-F: Cyclooctane. Side attached .....	49

Figure 2.4.42: Infrared Spectra Comparison (Cyclooctane Black, Li-Cyclooctane-F Blue, Li-F: Cyclooctane Red) ..... 51

Figure 2.4.43. Infrared Spectra Comparison (Cyclooctane Black, Li-Cyclooctane-F Blue, Li-F-Cyclooctane Red). Range 2750 cm-1- 3200 cm-1.).....51

## CHAPTER 4

Figure 4.1.1: 2D Self Assembled Network of Tetraoxane ..... 57

Figure 4.2.1: 2D C-C bonded Network of Tetraoxane ..... 58

## LIST OF ABBREVIATIONS AND SYMBOLS

BOA	Born-Oppenheimer Approximation
CHELPG	charges from electrostatic potentials using a grid-based method
D <sub>e</sub>	Dissociation energy
D	Debye
DID	dipole inside dipole
eV	electron volts
IR	Infrared spectroscopy
M	Alkali metals
Mol	insertion molecule
RS-PT	Rayleigh–Schrödinger Perturbation Theory
SCF	Self-Consistent Field
SD	Slater Determinant
TDSE	Time-Dependent Schrödinger Equation
TISE	Time-Independent Schrödinger Equation
X	reactive nonmetals
Å	Angstrom
$\hat{H}$	Hamiltonian operator
Pentaoxecane	1,3,5,7,9-Pentaoxecane

## **Chapter 1. Introduction**

### **1.1 Application**

The pursuit of discovering, designing, and studying new compounds and systems with novel and practical applications lies at the heart of chemical research. Polar systems offer a broad range of practical applications including, lasers and solar cells <sup>2, 3</sup>, nonlinear optics <sup>4</sup>, and ferroelectrics <sup>5</sup>. The study of polar systems has expanded over the past few years, with works including; optical properties of halogen cocrystals <sup>6</sup>, computational exploration of the halogen bond <sup>7</sup>,  $\pi$ -holes <sup>8</sup>, porous material penetration <sup>9</sup>, halogen/cocrystal bonding recognition <sup>10, 11</sup>. Previous studies have explored how counterions catalyze trapped-molecule isomerization <sup>12</sup>. In particular, polar molecules readily form complexes with alkali halides such as Li-F.

#### **1.1.1 Dipole moment**

The dipole moment is associated with the separation between positive and negative charges. An increase in the distance between two charges will increase the dipole moment. It is represented mathematically by the expression:

$$\mu = qd \quad (1.1.1)$$

Where  $\mu$  is the dipole moment,  $q$  is the magnitude charge difference, and  $d$  is the distance between the two charges. In particular, an increase in the dipole moment of an ion-pair can be achieved by stretching an ion pair (combination of positively and negatively charged species), this can be done by inserting a molecule in between the ion-pair.

### 1.1.2 Ion-pair trapping

Ion pair trapping, recognition, and reception have garnered significant interest over the past five years <sup>12-19</sup>. This field is expanding with potential applications in physiology, medicine, the environment, energy storage, and industrial manufacturing processes <sup>20</sup>.

A molecule inserted between stretched counterions characterizes ion-pair traps and prevents recombination of the counterions due to energy barriers. Two major factors contribute to the stability of these systems: the shape and the polarity of the inserted molecule. The structure, and composition of the insertion molecule affect the form of the electron density, which can have a concave shape in which the ion-pair will sit inside. A cyclic molecule provides this concave electron density to accommodate ion attachment (Figure 1.0). In this study, a cyclic molecule with a sufficiently large ring gap area has the potential for the ions to move through and penetrate. We examined the polarity of the ring-shaped cyclic molecule by comparing polar and nonpolar molecules. The molecule's polarity can facilitate ion attachment by attracting oppositely charged ions to the molecule, thereby trapping the molecule.

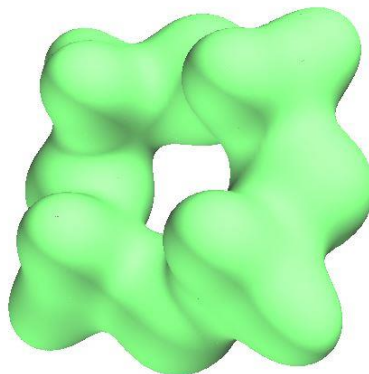


**Figure 1.0.** Electron density of Tetraoxane

Different ion pairs have a wide range of potential applications. In this work, the focus will be on Li-F. We selected Lithium for its intriguing use in energy storage as a mobile cation for electric cars and portable computing devices. Lithium is also used for its atom size, as it is the lightest and smallest metal. We selected Fluorine because of its relatively small atom size and strong bond with lithium; therefore, it is a good counterion for this computational study. Other ion pairs, such as Cs-Cl, Li-Cl, Li-I, Cs-F, and Cs-I, should be the subject of future studies. In many cases, larger cations can be used interchangeably with lithium. If complexes are meta-stable (negative  $D_e$ ) then energy could be stored at the molecular level.

### **1.1.3 Design of ring-shaped molecule and potential ion-pair traps**

Several factors aid in the attachment and stabilization effect of the ion pair when a molecule becomes trapped. These factors are hydrogen-bond donors, Lewis's acid sites, positively charged groups, Lewis base sites,  $\pi$ -electrons, and negativity-charged groups. These different groups form building blocks to help attract anions and cations and increase the stability of the complex after the ion pair has trapped the cyclic molecule.

The selection of molecules involves utilizing these building blocks and their properties to improve the molecule's ability to be a receptor of ions, increasing binding energies. It is preferable to select polar cyclic molecules as they can efficiently attract cations and anions simultaneously. In this work, two systems involve polar molecules, Tetraoxane and Pentaoxecane.

The cyclic molecules containing oxygen are chosen for their structure, having a concave electron density and polarity. Both characteristics positively affect how

the ion pairs are attached and trap the molecule. The oxygens are electron withdrawing, stabilizing the lithium cation. The hydrogens act as hydrogen-bond donors, stabilizing the fluorine anion. In this work, the organic structures have the oxygens grouped on one side of the cyclic molecule. This oxygen side of the system will carry a slightly negative charge (electron-rich), and the other side will be slightly positively charged or weak in electron density. This net difference in charge from one side of the molecule to the other gives this system a considerable dipole moment. These oxygen-enriched molecules act as a smaller dipole that sits inside the stretched dipole of Li-F. This dipole inside the dipole (dipole-in-dipole or DID) structure helps to stabilize the system by attracting positive cations to the negative portion of the molecule and the negative anions to the positive part. Figure 1.1 shows this stabilization effect.

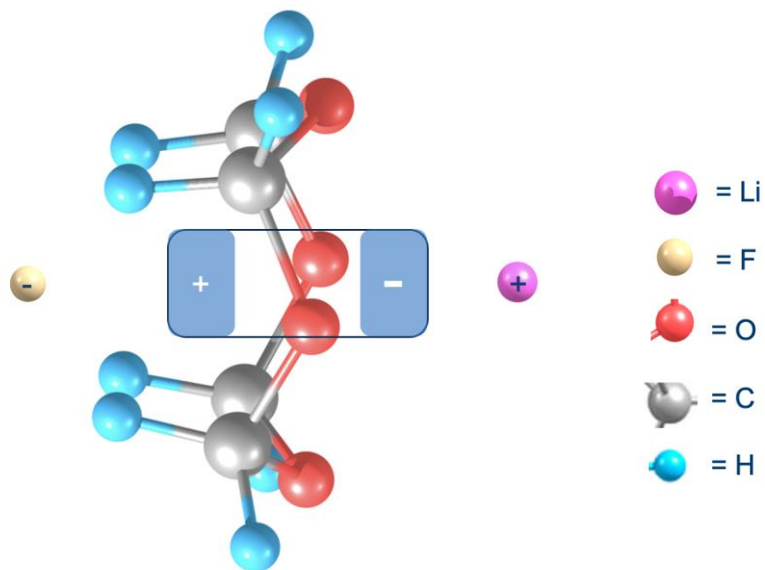


**Figure 1.1.** Dipole inside Dipole (F-Tetraoxane-Li).

The second interesting property of the design of ion-pair traps is a concave-shaped electronic density, similar to a “well”. This concave “well” increases the energy barrier for recollecting the ion pair around the molecule. This aspect favours the selection of cyclic molecules, as they naturally have concave-shaped electron

densities higher in the area around the ring and lower in the center. This “well” shaped cavity allows attaching ions to sit inside.

#### **1.1.4 Lithium penetrating**

Lithium penetrating through cyclic molecules of tetraoxane, pentaoxecane, and cyclooctane presents a novel aspect of this work. We examined two cases of lithium-ion penetrating. First is counter-ion assisted, where the fluorine counter-ion aids the lithium ion's passage across the ring. In the Second scenario, no counter-ion is utilized to help  $\text{Li}^+$ 's journey through the molecule's center. Lithium is an exciting ion to study because of its smaller size, which lowers the penetrating barrier compared to larger cations. We expect larger cations to have steric effects concerning penetrating; it is similar to pushing a progressively larger ball through a fixed circular hole. Larger ions will, therefore, have their equilibrium distance further from the molecule and increase the energy required for Penetrating.

#### **1.1.5 Ion-pair filtration**

Ion-pair binding is also of interest for ion removal or filtration. We can exploit the receptor's selectivity for binding to specific ions to remove the target ions from the aqueous phase. Carmeliet (1964)<sup>21</sup> controlled the receptor's selectivity with similar oxygen-embedded carbon rings, where 15-membered rings selectively bind with  $\text{NaCl}$ ,  $\text{NaBr}$ ,  $\text{NaNO}_3$ , and  $\text{NaNO}_2$ . Creating an organic phase rich with lithium-targeted organic ring receptors could purify an aqueous phase by removing targeted ions. This process leaves the desired ions untouched.

### **1.1.6 Analogous systems**

Ion pairs have trapped a series of halocarbons and hydrocarbons, for example;  $C_nH_nF_n$ <sup>15, 19</sup>, cyclic forms of  $C_nH_{2n}$  ( $n=3,4,6$ )<sup>13, 22-24</sup>,  $C_2F_6$ <sup>16</sup>, adamantane<sup>24</sup>, cubane<sup>12</sup>, and 1,3,5 trioxane<sup>18</sup>. In this work, the most similar polar and nonpolar cyclic molecules previously studied were the polar trioxane ( $C_3H_6O_3$ )<sup>18</sup> and nonpolar cyclohexane<sup>23, 24</sup>.

#### **1.1.6.1 Polar systems**

In this work, two polar systems, tetraoxane and 1,3,5,7,9-Pentaoxecane (Pentaoxecane), are larger cyclic molecules than the previously studied systems. We predict that a larger cyclic molecule could form more stable trapped complexes and be easier to penetrate by a cation. In the case of trioxane, the larger counter ion pairs explored were Na-Cl, Na-I, Cs-Cl, and Cs-I<sup>18</sup>. With the attachment of positive ions to the electronegative oxygen side, and negative ions are connected to the hydrogen side. Complexes of M-trioxane-X show a small positive Dissociation energy ( $D_e$ ) for all cases except Cs-Cl. These relatively small values are under 0.11 Electron Volts (eV)<sup>18</sup>. Sullivan<sup>18</sup> only reports energy barriers for Cs-trioxane-I and have approximately half an eV in height, keeping the M-mol-X complex together. The dipole moments of the M-trioxane-X systems show an increase in the dipole moment of 50% to 100% compared with free M-X<sup>18</sup>.

We previously studied  $C_4H_4F_4$  as another example of a polar cyclic molecule system combined with Cs-I as a trapping ion pair<sup>19</sup>. We examined two conformations of  $C_4H_4F_4$  for ion-pair insertion, all-cis and “cross”. All the fluorines are located on one side of the ring in the all-cis conformation, and in the ‘cross’ conformation, C<sub>1</sub> and C<sub>3</sub> carry the fluorines. The more polar all-cis geometry had a small positive  $D_e$  M-  $C_4H_4F_4$ -X compared to M-X +  $C_4H_4F_4$  after complexation, showing that stability is possible. The “cross” conformation had a negative  $D_e$  after complexation, leading to being meta-stable. An interesting point in this study was in the all-cis

conformation, and the framing ions helped flatten the ring in the Cs-C<sub>4</sub>H<sub>4</sub>F<sub>4</sub>-I system. The “cross” geometry does not exhibit this characteristic. The more polar all-cis conformation is higher in energy as a conformer, but complexes with ion pairs are more stable relative to Mol+M-X. This increase in stability is because the electro-negative side containing fluorines stabilizes the cesium cation, and the more positive hydrogen side helps stabilize the iodine anion. In the dipole moments of this study, we can see the effect of the dipole inside the dipole effect. The “cross” M-Mol-X complex has a more significant dipole moment than the all-cis by 50% <sup>19</sup>. This reduction in dipole moment is due to the system's polarity, the all-cis holds the ion-pair closer by approximately 1 Angstrom (Å), and its dipole moment counteracts the more significant dipole moment of the stretched ion-pair<sup>19</sup>.

All-cis C<sub>6</sub>H<sub>6</sub>F<sub>6</sub> is a larger polar cyclic molecule with fluorines on one side. It was studied computationally in <sup>16, 25</sup> and synthesized in <sup>26</sup>. M-X ion-pairs combined with it here are Cs-I and Cs-Cl. Here, complexes M-C<sub>6</sub>H<sub>6</sub>F<sub>6</sub>-X have positive D<sub>e</sub> values M-Mol-X compared to M-X + Mol. Thus, M-mol-X complexes are lower in energy than Mol+M-X separate, indicating their stability<sup>16</sup>. This stability comes from the significant dipole moment of the ring. This system does have the ring flattening effect similar to that of all-cis C<sub>4</sub>H<sub>4</sub>F<sub>4</sub> mentioned previously, with alterations to the cyclic molecule limited to under 0.05 Å<sup>16</sup>.

#### 1.1.6.2 Nonpolar Systems

C<sub>6</sub>H<sub>12</sub> cyclohexane has a nonpolar ring structure that has been previously studied. It was discovered to form trapped M-Mol-X complexes with M-X ion pairs of Cs-I and Cs-Cl<sup>16, 27</sup>. Complexes of Cs-cyclohexane-I are not stable and have a negative value of D<sub>e</sub>. These complexes also have low 0.1 eV barriers preventing recombination of ion-pair around the molecule. These properties indicate that these complexes are metastable systems (negative D<sub>e</sub>), and short-living (low barriers for recombination). M-C<sub>6</sub>H<sub>12</sub>-X systems have a more significant dipole moment than similar M-C<sub>6</sub>H<sub>6</sub>F<sub>6</sub>-X. Lower stability and larger dipole moment are due to the lack

of a dipole inside dipole effect. Without this DID effect, there is no force stabilizing the ions and no dipole counteracting the dominant dipole moment of the stretched ion-pair. An interesting point here is that M-X ions do not sit on a line that passes through the center of the ring in complexation. This could result from two factors: the size of the ions, and the size of the ring. We predict that a larger ring with smaller ions will form a stable M-Mol-X complex more effectively because of its increased “well” shape.

Two C<sub>8</sub>H<sub>8</sub> isomers; cubane and 3-ladderene, are nonpolar systems studied with Li-F as counter ions to form insertion complexes <sup>12</sup>. These nonpolar cyclical molecules form complexed systems that are metastable with negative values of D<sub>e</sub>. These systems could be short-lived, having less than half eV barriers that keep the M-Mol-X complex together, preventing M-Mol-X recombining to Mol+M-X <sup>12</sup>. The dipole moments are prominent in these systems, with a 2.5 times higher value of dipole moments than in individual free ion-pair systems <sup>12</sup>. Similar to the previous case, this results from the missing DID effect, increasing stability and reducing the overall dipole moment of the complexes formed.

C<sub>4</sub>H<sub>8</sub> cyclic molecule system was studied for insertion complexes with the M-X ion pairs, Li-Cl, Li-I, Cs-Cl, and Cs-I <sup>13</sup>. All M-C<sub>4</sub>H<sub>8</sub>-X systems are metastable, having negative D<sub>e</sub> values of M-Mol-X compared to Mol+M-X <sup>13</sup>. In such complexes with substantial charge transfer, the flattening of the cyclic molecule is more pronounced <sup>13</sup>. Will smaller ion pairs, such as Li-F, be able to flatten larger cyclic molecules? Small energy barriers of 0.2 eV <sup>13</sup> preventing recombination of the ion pair are partly attributed to the relaxation of the ring back to a bent geometry. Adamantane and cyclohexane were studied with the Li-F ion pair for complexation and lithium penetrating <sup>24</sup>. One larger nonpolar cyclic molecule, cyclooctane, was studied in this work.

### **1.1.7 Infrared spectroscopy (IR)**

IR spectroscopy (spectra) is a powerful analytical technique used to help identify functional groups in a molecule based on its vibrational modes with the absorption of infrared light. Each functional group in a molecule has its own characteristic set of vibrational modes that result in unique IR absorptions. These absorptions appear as peaks in the IR spectrum, and their position, intensity, and shape can provide valuable information about the chemical structure of a molecule. Researchers can use these IR spectra data to distinguish conformations when synthesizing them.

## **1.2 Thesis Objectives**

The Li-F ion-pair's ability to trap, attach to, and penetrate through the cyclic molecules tetraoxane, pentaoxecane, and cyclooctane was explored. We studied both polar molecules (tetraoxane/pentaoxecane) and nonpolar molecules (cyclooctane) to compare how the polarity of the molecules affects the structure and stability of the formed complexes. We determined properties such as  $D_e$ , geometry, charges, and dipole moments. We calculated IR spectra to help identify if the synthesis of these systems is achieved, distinguishing each conformation from another.

Energy barriers for  $\text{Li}^+$  and  $\text{F}^-$  ions to recollect around the cyclic molecules after complexation were calculated, and these will indicate the stability of the Li-Mol-F complex formed. The energy barrier for the  $\text{Li}^+$  cation to penetrate each of the cyclic molecules, both assisted by  $\text{F}^-$  on the other side and unassisted were calculated, to compare the effect of a counter ion on  $\text{Li}^+$ 's penetrating. Two body systems, M-Mol and Mol-X, were also studied to understand ion attachment energies and possible complex formation pathways.

## **Chapter 2. Body of thesis**

### **2.0 Methods**

#### **2.1 Computational Chemistry**

Computational Chemistry can trace its origins back to the 1920s with publications by Heisenberg<sup>28</sup>, Schrödinger<sup>29</sup> and Huckel's theory of Pi electrons<sup>30</sup>. Modern computational chemistry began with the first software becoming available in the 1950s, with the advancement and development of theoretical models. Interest in the field grew with computational chemistry, able to solve different chemical properties, structures, and geometries. Many textbooks<sup>31-34</sup> that report on the advancement of the area are readily available. Therefore, this section provides a brief history and lays the foundation for understanding the field. This section will also give a brief history of the field of computational chemistry for those who are not familiar with it.

Computational chemistry is a rapidly evolving interdisciplinary field that combines many elements from theoretical chemistry, computer science, and quantum mechanics. We use it to understand and explore molecular systems and their properties. The area of computational chemistry uses mathematical models and simulations to provide insight into a material's structure, energy, reactivity, and polarity and predict spectroscopy results. These insights enable the prediction of chemical behaviour and help design new materials, drugs, or chemicals.

Quantum mechanics is the fundamental theory that describes the behaviour of matter at the atomic scale. Quantum chemistry is a subfield of computational chemistry that uses quantum mechanical methods to model chemical systems<sup>31</sup>.

In drug discovery, computational chemistry is used for identifying potential drug candidates and optimizing lead compounds, making it one of the exciting applications of this discipline. It is employed to predict the pharmacokinetics and toxicological properties <sup>35</sup>. Computational chemistry was used at the onset of the covid 19 pandemic to map the shape of the virus to other known viruses to start drug discovery and modifications of existing drugs that could more closely bind to the COVID-19 virus for insights on how to treat it <sup>36</sup>. In materials science, computational chemistry is also used to aid in designing and discovering novel materials with exciting properties/materials/systems, such as catalysis, polymers, energy storage, nanomaterials, ion-pair receptors, ion traps, supramolecular complexes, significant dipole moments, charge transfer, non-covalent interactions, and ion penetrating <sup>12-15, 18-20, 24, 37, 38</sup>.

### 2.1.1 Schrödinger equation

The Schrödinger equation commands the wave function of a quantum system. Austrian physicist Erwin Schrödinger formulated it in 1925, published it in 1926, and was the groundwork for the Nobel Prize in 1933. It is a cornerstone of quantum mechanics that has revolutionized our understanding of the microscopic world. This equation provides the backbone of the mathematical framework for describing particles' wave-like properties and behaviours. The Schrödinger equation has been instrumental in elucidating numerous phenomena in physics, chemistry, and materials science and has led to remarkable advancements in these fields.

The first form of the Schrödinger equation is the time-dependent Schrödinger equation (TDSE), which describes the time evolution of a given quantum system's wave function and is described by:

$$\hat{H}\psi(x, t) = i\hbar(\partial\psi(x, t)/\partial t) \quad (1.0)$$

$\hat{H}$  is the Hamiltonian operator, which represents the system's total energy,  $\Psi(x, t)$  is the wave function of the system as a function of position (x) and time (t), and  $\hbar$  is the reduced Planck constant.

The second form of the Schrödinger equation is the time-independent Schrödinger equation (TISE). The TISE is commonly used to analyze stationary states and energy levels of given quantum systems <sup>32</sup> and is displayed as follows:

$$\hat{H}\psi(x) = E\psi(x) \quad (1.1)$$

Where  $\hat{H}$  is the Hamiltonian operator,  $\Psi(x)$  is the time-independent wave function of the system as a function of position (x), and E is the energy eigenvalue corresponding to the eigenstate  $\Psi(x)$ .

Solving the Schrödinger equation yields essential information about the system's behaviour, including energy levels and wave functions <sup>33</sup>.

### 2.1.2 Hamiltonian operator

The Hamiltonian operator ( $\hat{H}$ ) is a central element in the Schrödinger equation. Its primary purpose is to describe a quantum system's total energy, including its kinetic and potential energy components. The typical form of the Hamiltonian operator that concerns this work considers five contributions to the total energy of a quantum system <sup>34</sup>: the kinetic energies of the electrons and nuclei, the coulombic attraction energy of the electrons to the nuclei, the energy of electron-electron/nucleus-nucleus repulsions which are described as follows:

$$\hat{H}\Psi = -\sum_i \frac{\hbar^2}{2m} \nabla_i^2 \Psi - \sum_k \frac{\hbar^2}{2m_k} \nabla_k^2 \Psi - \sum_{i,k} \frac{e^2 Z_k}{r_{ik}} \Psi + \sum_{ij} \frac{e^2}{r_{ij}} \Psi + \sum_{kl} \frac{e^2 Z_k Z_l}{r_{kl}} \Psi \quad (1.2)$$

where  $m$  is the particle's mass,  $\nabla^2$  is the Laplacian operator,  $Z$  is the charge of a nucleus,  $i$  and  $j$  are the indexes of electrons,  $k$  and  $l$  are the index of nuclei,  $\hbar$  is Planck's constant divided by  $2\pi$ ,  $r_{ab}$  is the distance between two particles  $a$  and  $b$ , and  $e$  is the charge of a proton.

### 2.1.3 Born-Oppenheimer Approximation

Born and J. Robert Oppenheimer introduced the Born-Oppenheimer approximation (BOA) in 1927. This approximation offers a simplified framework for studying molecular systems <sup>39</sup>. This approximation relies on the assumption that the motion of the nuclei in a molecule can be separated from the movement of the electrons. This assumption is grounded in the significant mass difference of electrons and nuclei (made of up protons and neutrons), in that protons and neutrons are approximately 1800 times more massive than electrons <sup>34</sup>. This mass difference is reflected in the kinetic portions in equation 1.2 (Hamiltonian operator), and for practical purposes, electron ‘relaxation’ concerning nuclei motion can be considered instantaneous <sup>40</sup>.

Consequently, the nuclear and electronic degrees of freedom can be treated independently. The BOA significantly simplifies the Schrödinger equation for molecular systems. After the BOA has been applied to equation 1.2, we arrive at the more straightforward equation, where the kinetic energy of the nuclei term goes to 0, and the repulsive nucleus-nucleus term is now constant for a given geometry:

$$\hat{H}\Psi = -\sum_i \frac{\hbar^2}{2m} \nabla_i^2 \Psi - \sum_{i,k} \frac{e^2 Z_k}{r_{ik}} \Psi + \sum_{ij} \frac{e^2}{r_{ij}} \Psi + \sum_{kl} \frac{e^2 Z_k Z_l}{r_{kl}} \Psi \quad (1.3)$$

Using the BOA enables us to separate the molecular wave function into two distinct and simpler parts: the electronic and nuclear wave functions. The electronic

wave function is dependent on the position of electrons, and the nuclei wave function is dependent on the position of the nuclei. By utilizing the BOA, the calculations are simplified, making studying bigger and more complex molecular systems possible. This approximation is the foundation of most quantum chemistry methods, such as density functional theory (DFT), and ab initio methods, such as Hartree-Fock.

#### **2.1.4 Hartree-Fock Self-Consistent Field Method**

The Schrödinger equation describes a concept in quantum systems where each single electron interacts with all other electrons in the system and, as a result, depends on all other electrons. With this approach, the Schrödinger equation for many bodies cannot be exactly solved, therefore an approximation is required to solve it. Simplifications are done to the many-electron system to give us an approximation. One such approximation is that of the Self Consistent Field Hartree-Fock (SCF-HF). SCF-HF uses a single Slater determinant to obtain ground-state wave functions iteratively.

These approximations have drawbacks regarding their accuracy compared to real systems. In SCF-HF, a single Slater Determinant (SD) approximation is used. Single-determinate approximations are insufficient in calculations where multiple orbitals are degenerate. This effect is called “Non-Dynamical Correlation”<sup>41</sup>.

With SCF-HF, the most significant errors come from neglecting the Electron Correlation. These errors arise from treating electron-electron interaction as the average effect between electrons in the system. These interactions are coulombic in that when one of the electrons moves, all others are affected, i.e. with no independent movement.

### **2.1.5 Møller Plesset Perturbation Theory**

Christian Møller and Milton S. Plesset Møller-Plesset introduced the Perturbation Theory in their seminal paper published in 1934<sup>42</sup>. They proposed an approximation treatment for the many-electron systems based on the Rayleigh-Schrödinger Perturbation Theory in that paper. In this method, they expand the system's total wave function and energy as a power series. Perturbation theory, applied to an electronic structure with Hartree-Fock as an unperturbed solution, is called Møller-Plesset Perturbation Theory (MPPT)<sup>42, 43</sup>. Møller-Plesset Perturbation Theory uses the Fock operator (Fock operator is a one-electron operator, therefore will not contain electron correlation) as the unperturbed Hamiltonian, with electron correlation effects accounted for utilizing Rayleigh–Schrödinger Perturbation Theory (RS-PT).

Over the years, researchers have further developed MPPT, with the second-order Møller-Plesset Perturbation Theory (MP2) being the most common and widely used version. The research in this thesis operates at the MP2 level of accuracy. MP2 significantly enhances the Hartree-Fock (HF) method by incorporating electron correlation effects, which are essential for accurate descriptions of molecular properties and energetics<sup>44</sup>. The MPPT approach has also been extended to higher orders (MP3, MP4, etc.), providing even more accurate results concerning electron correlation but at a higher computational cost<sup>45</sup>. These higher-level calculations were not selected because MP2 gives good comparison to experimental results and because of their significantly higher cost of computing, increasing the length of calculations outside the project's time constraints.

With the exact Hamiltonian ( $\hat{H}$ ), the unperturbed Hamiltonian ( $\hat{H}^0$ ), and the perturbation  $V$ , the relationship between them is as follows:

$$\hat{H} = \hat{H}^0 + V \quad (1.4)$$

Rearranged, we can see that in MPPT, the perturbation  $V$  is the difference between the exact electron-electron interactions and the average electron-electron interactions in HF:

$$V = \hat{H} - \hat{H}^0 \quad (1.5)$$

Starting with 0<sup>th</sup> order,  $H_0$  is the sum of the one-electron Fock operators from the Hamiltonian after the BOA has been applied. This is the approximate Hamiltonian or 0<sup>th</sup> order:

$$\hat{H}^0 \Psi^0 = E^0 \Psi^0 \quad (1.6)$$

There is an error in equation 1.6, regarding  $E^0$  where each orbital energy includes the electron-electron repulsions with respect to all of the other electrons. Therefore, the electron-electron repulsions will be overcounted twice, once in each pair, for example,  $e_1$  interactions with  $e_2$ , and again with  $e_2$  interacting with  $e_1$ . We must move on to the next order in MPPT to fix this.

The 1<sup>st</sup> order MP can be expressed as follows:

$$E = E^0 + E^1 \quad (1.7)$$

Where the energy  $E$  is equal to the unperturbed energy  $E^0$  plus the 1<sup>st</sup> order correction  $E^1$ . This 1<sup>st</sup> order correction is expressed by:

$$E^1 = \langle \Psi^0 | V | \Psi^0 \rangle \quad (1.8)$$

$\langle \rangle$  is bra-ket notation invented by Paul Dirac<sup>46</sup>, and is used in quantum mechanics to express operators in complex vector spaces more simply. Here this indicates integrating over the change in the space due to the perturbation  $V$ . Solving for  $E$  in MP<sub>1</sub> (equation 1.7) reproduces HF, with its correct values of overcounting. Therefore, to obtain improvements, we must move on to MP<sub>2</sub>. We need to add a term to equation 1.7 to account for the adjustments to be made in this 2<sup>nd</sup> order calculation, which can be written as follows:

$$E = E^0 + E^1 + E^2 \quad (1.9)$$

Where the energy  $E$  is equal to the unperturbed energy  $E^0$ , plus the 1<sup>st</sup> order correction  $E^1$ , and with the addition of the 2<sup>nd</sup> order correction  $E^2$ . The 2<sup>nd</sup> order correction  $E^2$  can be expressed by :

$$E^2 = \sum_{n \neq 0} \frac{|\langle \Psi_n^0 | V | \Psi^0 \rangle|^2}{E^0 - E_n^0} \quad (1.10)$$

We can now solve for an energy for the 2<sup>nd</sup> order calculations or MP<sub>2</sub>. With  $E=E^0+E^1+E^2$  equation 1.9, an approximate energy can be found that improves on HF<sup>32</sup>. This expansion can continue beyond MP<sub>2</sub> to MP<sub>3-6</sub>; if this series converges, it will converge at the actual energy value. However, these expansions have a significantly increased computing cost and will not be done in this work. The MP<sub>2</sub> method has the benefit of accounting for electron-electron correlation compared to HF, where it is not considered.

## 2.2 Methods

We have performed calculations at the MP2 level of theory, using the extensive aug-cc-pVDZ basis sets for hydrogen, carbon, oxygen, lithium, and fluorine atoms.<sup>47</sup> We chose this level as a reasonable compromise between accuracy and computation time. It is also suitable for systems of this size, which involve noncovalent interactions and significant charge transfer. This is supported by comparing the calculated and experimental parameters for the ion-pair Li-F shown in Table 2.1, with deviations within 10% regarding  $D_e$ , 3% in equilibrium distance, and 3% in dipole moment. Other Diatoms, Li-H, H-F, Li-O, and O-F are also included. We included these because, in complexation, they are the closest atoms to the interacting atom pairs in the study and are relevant for comparison.

**Table 2.1.** Equilibrium parameters of Li-F (In brackets are experimental values<sup>1</sup>).

System	$D_e$ (eV)	$R_e$ (Å)	$\mu$ (D)
Li-F	6.13 (5.98)	1.61 (1.56)	6.50 (6.33)
Li-H	2.24 (2.47)	1.62 (1.60)	6.00 (5.88)
H-F	6.23 (5.91)	0.93 (0.92)	1.82 (1.83)
Li-O	3.50 (3.37)	1.70 (1.69)	6.45 (6.84)
O-F	1.90 (1.83)	1.34(1.35)	0.06 (0.00)

We employed the NWChem Quantum Chemistry Package<sup>48</sup> for the specified ab initio computations. To confirm the presence of local minima of energy or a transition state, we followed all-atom unconstrained optimizations from the initial geometries and conducted vibrational frequency analysis. The transition-state geometries (geometries with imaginary frequencies) have been edited in accordance with the normal-mode vectors and reoptimized as required. We evaluated energy

barriers in various ways where applicable. In the most straightforward cases, we assessed them through a series of fixed displacements along the reaction pathway while optimizing the rest of the system. In other cases, the bond angle or dihedral angle is varied to rotate lithium or fluorine around the edge of the cyclic molecule to recollect on the other side. In  $\text{Li}^+$  penetrating barriers, we positioned neon at a fixed point away from the molecule, and  $\text{Li}^+$  would be moved towards it, fixing the bond distances  $\text{Li}^+ \text{-Ne}$ . We obtained atomic charges using the CHELPG (CHarges from Electrostatic Potentials using a Grid-based) method<sup>49</sup>, where atomic charges are fitted to the molecular electrostatic potential at varying points around the system <sup>34</sup>.

To validate the IR-Spectra that is produced by NWChem a comparison to experimental spectra<sup>50</sup> was done (Figure 2.1.1). An agreement of the two spectra can be seen with peaks in the  $500\text{-}1500\text{ cm}^{-1}$  range, and slight blue-shifting of the peak around  $3000\text{cm}^{-1}$ .

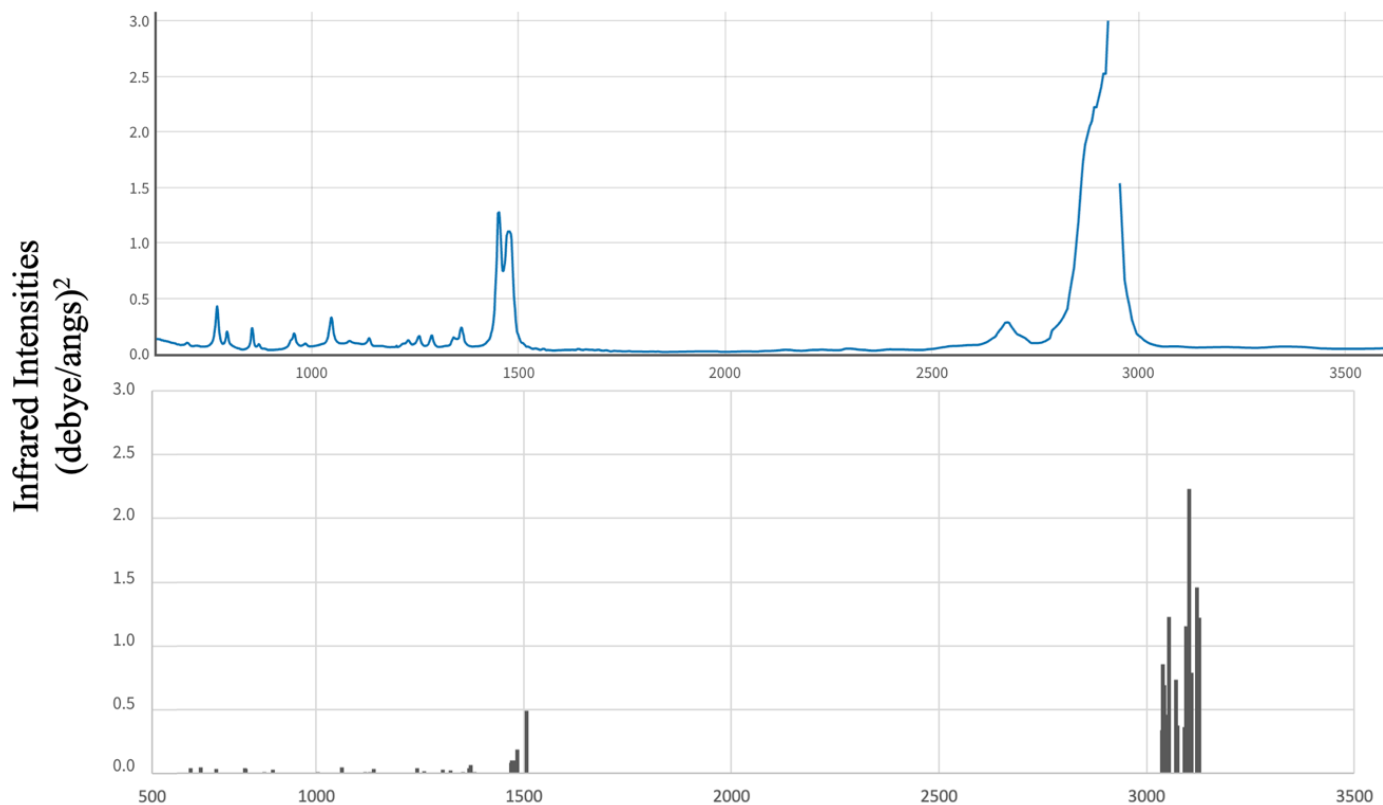


Figure 2.1.1: Comparison of Experimental and Calculated Infrared Spectra for Cyclooctane (experimental top / Calculated Below)

## 2.3 Results

**Table 2.2.** Energies, internal distances, and dipole moments. \*For Tetraoxane (Flipped) systems Li-H and O-F distances are listed.

System	Dissociation Energy $D_e$ (eV)	$R_e$ (Li-O) (Å)	$R_e$ (H-F) (Å)	Li-F distance (Å)	Dipole Moment (D)
Tetraoxane					3.64
Li-Tetraoxane-F	0.38	2.03	1.88	4.06	6.94
F-Li-Tetraoxane	1.11	2.19		1.62	11.56
Tetraoxane-F-Li	1.12		2.35	1.61	11.61
$\text{Li}^+$ -Tetraoxane	5.89	2.15			
Tetraoxane-F <sup>-</sup>	1.52		2.05		
Tetraoxane-F	0.04		3.07		3.76
F-Tetraoxane-Li	-4.98	1.87*	2.71*	4.61	17.23
F <sup>-</sup> -Tetraoxane	-1.52		2.06*		3.570
Tetraoxane-Li <sup>+</sup>	0.151	2.03*			
Cyclooctane					0.080
Li-Cyclooctane-F	-2.04	2.03	1.80	4.16	10.74
F-Li: Cyclooctane	0.56	1.92	2.50	1.61	6.07
Cyclooctane: F-Li	0.56	1.92	2.50	1.61	6.08
$\text{Li}^+$ -Cyclooctane	1.46	2.13			
Pentaoxecane					4.40
Li- Pentaoxecane -F	1.13	1.89	1.92	3.71	4.36
F-Li-Pentaoxecane	1.38	2.07		1.64	12.31
F-Li: Pentaoxecane	1.29	1.91	2.34	1.62	4.98
$\text{Li}^+$ -Pentaoxecane	3.86	1.92			1.19
Pentaoxecane-F <sup>-</sup>	1.76		2.08		1.44

**Table 2.3.** Ring gap area.

System	Area of Gap ( $\text{A}^2$ )
Tetraoxane	5.68
Li-Tetraoxane-F	5.49
Cyclooctane	6.71
Li-Cyclooctane-F	7.14
Pentaoxecane	8.61
Li-Pentaoxecane-F	8.72

The ring gap area is approximated geometrically, dividing the area made by the oxygen/carbons on one side of the cyclic molecule into triangles. This underestimates the area but gives a comparison between systems.

**Table 2.4.** Charges from Electrostatic Potentials

	CHELPG ESP		
	q(Li)(e)	q(F)(e)	q(Mol)(e)
Tetraoxane			
Li-Tetraoxane-F	0.827	-0.751	-0.076
Li-F-Tetraoxane	0.792	-0.864	0.072
Tetraoxane-Li-F	0.827	-0.751	-0.076
Tetraoxane: Li-F	0.794	-0.861	0.067
F-Tetraoxane-Li	0.348	-0.331	-0.017
Cyclooctane			
Li-Cyclooctane-F	0.775	-0.847	0.072
Li-F: Cyclooctane	0.735	-0.812	0.076
Pentaoxecane			
Li- Pentaoxecane -F	0.800	-0.714	-0.086
F-Li- Pentaoxecane	0.676	-0.851	0.174
F-Li:Pentaoxecane	0.809	-0.840	0.031

## 2.4 Discussion

In this discussion, we delve into the exploration of Li-F ion-pair interactions with cyclic molecules scrutinizing their ability to trap, adhere to, and penetrate these molecular structures. Our investigation encompasses both polar (tetraoxane/pentaoxecane) and nonpolar (cyclooctane) molecules, illuminating the impact of polarity on the structure and stability of resulting complexes.

### 2.4.1 Tetraoxane

The tetraoxane molecule (Figure 2.4.1) is a cyclic molecule consisting of alternating CH<sub>2</sub> groups and oxygen atoms. The oxygen and carbon atoms are located

in different planes, which creates an appreciable dipole moment of 3.64 D (table 2.2) across the molecule (Scheme 2.4.1). This dipole moment facilitates ion attachment, and this ion-dipole attraction is a contributing factor to the stability of the Li-Tetraoxane-F complex (Figure 2.4.2) which has a dissociation energy ( $D_e$ ) of 0.375 eV (Table 2.2) relative to Li-

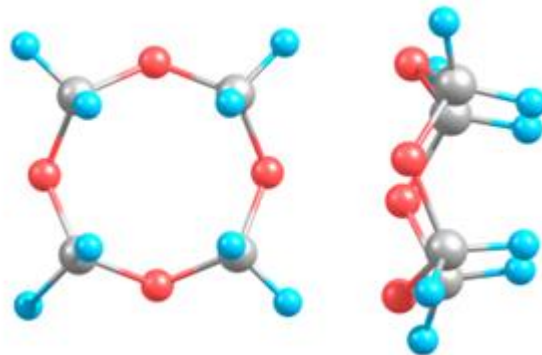


**Figure 2.4.1.** Tetraoxane. Front view (Left) Side View (Right).

F + Tetraoxane. The electronegativity of oxygen is the most significant contributing factor to this force.

Relaxed Li<sup>+</sup>-Tetraoxane (Figure 2.4.3) and Tetraoxane-(F<sup>-</sup>) (Figure 2.4.4) generally have structures similar to those in the trapped complex, with ions slightly farther away from tetraoxane (Table 2.2). This increased M-mol distance is due to the missing attracting

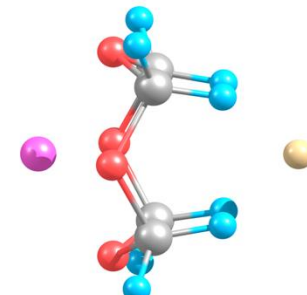
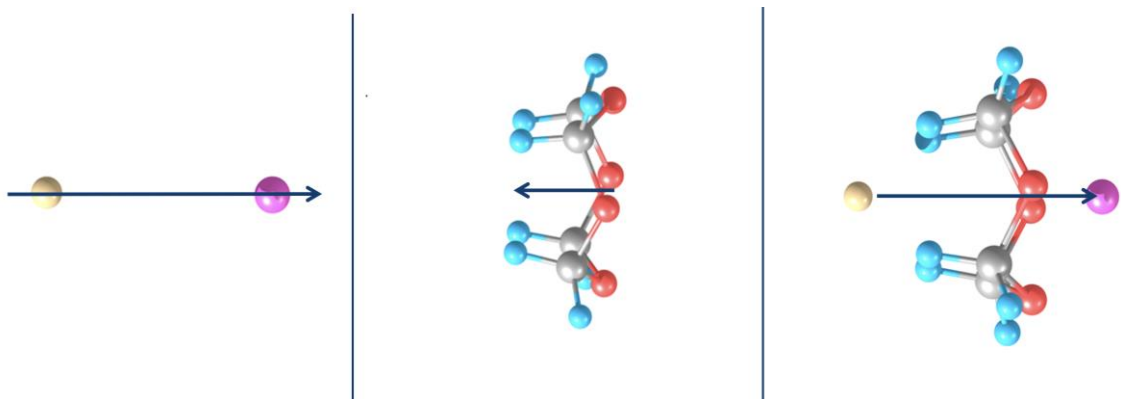


**Figure 2.4.2.** Li-Tetraoxane-F complex.

force of the counterion on the other side of tetraoxane.  $\text{Li}^+$  sits close to the electronegative oxygens, with  $\text{F}^-$  in the opposite position close to the positive hydrogens.



**Scheme 2.4.1:** Dipole components of Li-Tetraoxane-F complex. Li-F (Left), Tetraoxane (middle), Li-Tetraoxane-F (Right)

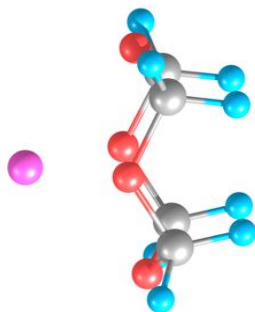


**Figure 2.4.3.** Tetraoxane-( $\text{Li}^+$ ). Tetraoxane has a considerable attachment energy of  $\text{Li}^+$  at 5.89 eV. Two factors impact this attachment energy, first  $\text{Li}^+$  significant charge density results in polarizing of the mol. Secondly, the electronegativity of oxygen is a contributing factor to this difference in attachment energy compared to non-polar systems. Oxygen is significantly electronegative and contributes to the polarity of tetraoxane. This is the largest attachment energy of  $\text{Li}^+$  in this work and is significantly larger than that of analogous systems, such as ( $\text{Cs}^+$ )-Trioxane, where the ion attachment energy is 0.97 eV<sup>18</sup>, and in ( $\text{Cs}^+$ )-BzO<sub>3</sub>, where the ion attachment energy is 1.58eV<sup>17</sup>, in the polar cyclic molecule C<sub>6</sub>H<sub>6</sub>F<sub>6</sub>, the  $\text{Cs}^+$  ion has an ion attachment energy limited to 1.24 eV ( $\text{Cs}^+$ -C<sub>6</sub>H<sub>6</sub>F<sub>6</sub>)<sup>16</sup>. Non-polar systems have also been studied, with  $\text{Li}^+$  ion attachment energies much weaker compared to our system but comparable to that of larger ions in analogous systems, such as 1.09 eV in ( $\text{Li}^+$ )-Cubane and 1.50 eV in ( $\text{Li}^+$ )-Ladderene. Lithium has a stronger attachment force than the larger cesium, which could be due to its more significant charge density. This strong attachment energy can help facilitate complexation by the

stepwise pathway of having  $\text{Li}^+$  ion attach first, with  $\text{F}^-$  ion attaching on the other side afterwards.

$\text{F}^-$  ion has an attachment energy of 1.52 eV, which is significantly less than the  $\text{Li}^+$  ion's attachment energy. In Trioxane<sup>18</sup>, this trend of  $\text{X}^-$  being lower in attachment energy than  $\text{M}^+$  is also seen, this could be explained by the charge density of smaller ions. This value of attachment energy is comparable to values found for  $\text{Cl}^-$  attachment energy to  $\text{C}_6\text{H}_6\text{F}_6$  at 1.80 eV<sup>16</sup>, in this case, values for  $\text{M}^+$  and  $\text{X}^-$  ( $\text{Cs}-\text{Cl}$ ) are close this could be because of the relative size of the ions in the pair. Lithium is very small, and fluorine is three times larger in size. This size difference allows lithium's charge density to be higher, attaching more deeply. In cases where the  $\text{Cs}-\text{I}$  ion pair is larger in size but with  $\text{M}^+$  attachment energy being higher than respective  $\text{X}^-$ , in this case,  $\text{Cs}^+$  is higher in attachment by 30% than  $\text{I}^-$ <sup>17</sup>.

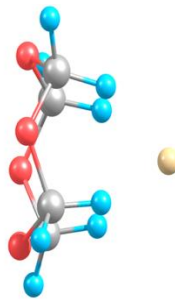


**Figure 2.4.4.** ( $\text{F}^-$ )-Tetraoxane.

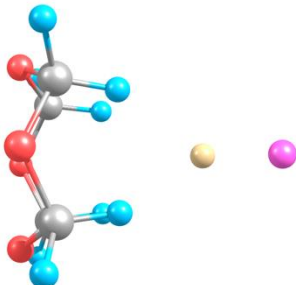


**Figure 2.4.5.** Tetraoxane- $\text{F}-\text{Li}^+$ .  
(F point.)

After complexation, the Li-F bond distance (in Li-Mol-F) is stretched to 4.06 Å compared to 2.01 Å in free Li-F. This stretch is associated with an increased dipole moment to 6.94 D (Li-Mol-F) from 6.50D (Free Li-F). Once this complex is formed, energy barriers keep it together, we explored four energy barriers. The first energy barrier is described as F moving along its pathway around tetraoxane. This barrier is shown in (Figure 2.4.6) and has a height of 1.81 eV. Lithium has two energy barriers, the first is shown in (Figure 2.4.6), here in this energy barrier, lithium moves around to recollect with fluorine on the other side and has a height of 1.73 eV. The tetraoxane ring is wide enough for lithium to slip through and can be assisted by  $F^-$  in the Li-Mol-F case or unassisted in the  $Li^+$ -Mol case. By comparison, in the  $Li^+$ -Tetraoxane case, the unassisted  $Li^+$  penetrating barrier (in the absence of  $F^-$ ) is 6.97 eV (Figure 2.4.7). This Penetrating barrier is reduced when fluorine helps pull Li through, to 2.75 eV. This represents a 61% reduction in barrier height, which is a significant reduction in the barrier for penetrating.

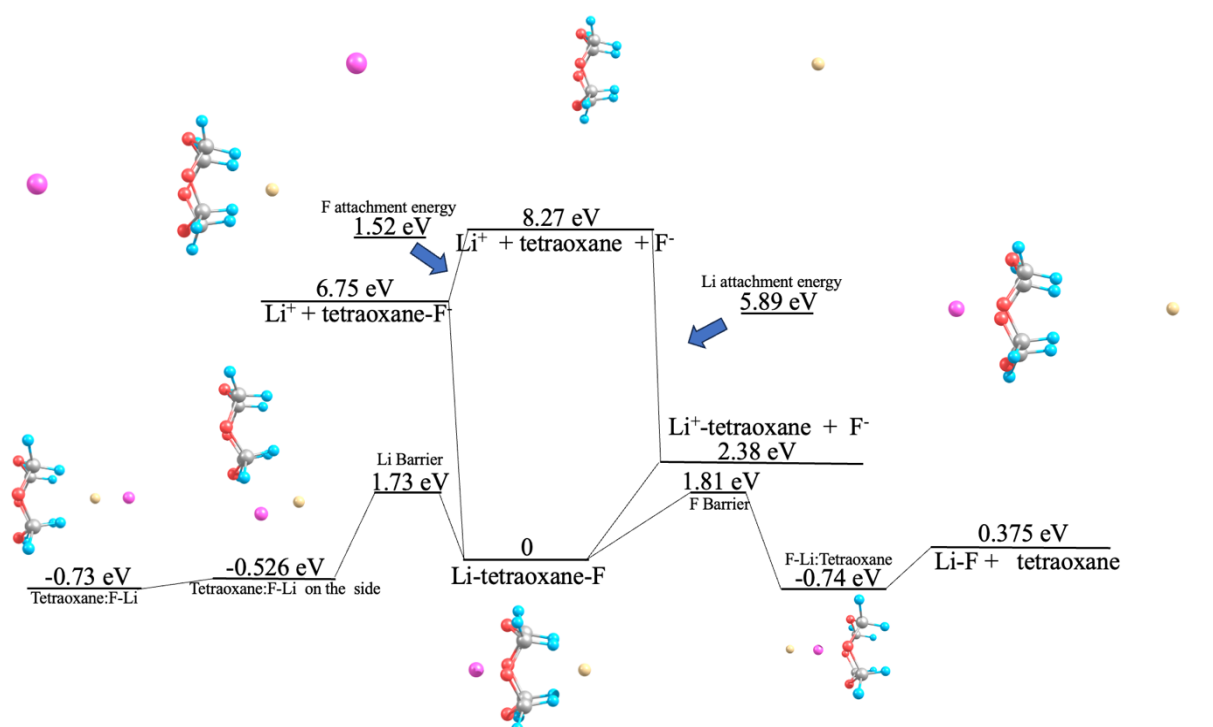


**Figure 2.4.6.** Tetraoxane Complex Energy Diagram.

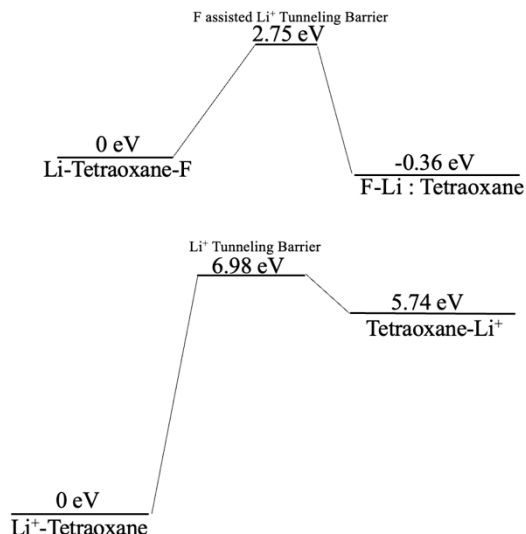


**Figure 2.4.7.** Tetraoxane  $\text{Li}^+$  Penetrating Energy Barriers

$\text{F-Tetraoxane-Li}$ , shown in Figure 2.4.8 is an interesting geometry. It has  $\text{Li-F}$  flipped around and attached in the energetically less favorable direction, with lithium on the positive side and fluorine on the negative side. This flipped  $\text{F-Tetraoxane-Li}$  system has a dissociation energy of -4.98 eV relative to  $\text{Li-F+Tetraoxane}$  and is the highest energy metastable system found. Interestingly, it has a huge dipole moment of 17.234 D, the largest dipole moment found in this study. This dipole is mainly due to the additive effect of the dipole moment of the Tetraoxane and ion pair's increased bond distance at 4.608 Å (compared to that of 4.06 Å in  $\text{Li-Tetraoxane-F}$ ).

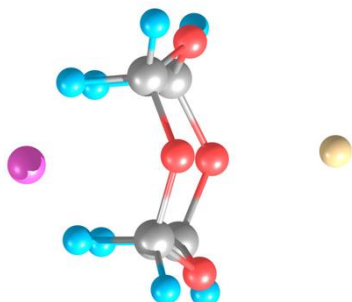


**Figure 2.4.8.**  $\text{F-Tetraoxane-Li}$ .  
(Flipped)

For the flipped F-Tetraoxane-Li system two energy barriers that keep this meta-stable complex together (Figure 2.4.10). The first barrier is that for F travelling around tetraoxane, it is 2.92 eV in height. The second is for Li travelling around tetraoxane, which is 2.89 eV in height. The Li barrier is slightly smaller and, thus is the more likely barrier that will be overcome for the recombination of ions. These barriers are quite high for a meta-stable complex, indicating that this interesting system is possible. In the flipped case, Tetraoxane-Li<sup>+</sup> (Figure 2.4.9) has an attachment energy of 0.151 eV, indicating that it is only weakly stable. This attachment energy is due to the repulsion effect of Li<sup>+</sup> sitting on the positive hydrogen side of the molecule. We studied two Li<sup>+</sup> Penetrating energy barriers for the flipped F-Tetraoxane-Li systems (Figure 2.4.11). First we have the F<sup>-</sup> assisted barrier at 0.93 eV in height and second the Li<sup>+</sup> unassisted barrier of 1.24 eV in height. Interesting here the unassisted barrier for the flipped Tetraoxane-Li<sup>+</sup> is significantly lower than in the Li<sup>+</sup>-Tetraoxane case, this indicates an energetic favoring of one direction (Tetraoxane-Li<sup>+</sup> => Li<sup>+</sup>-Tetraoxane). This can be explained by the Li<sup>+</sup> ion being pulled/assisted to the other side by the polarity of Tetraoxane, where this would be reversed for the opposite direction (hindering Li<sup>+</sup> Penetrating).

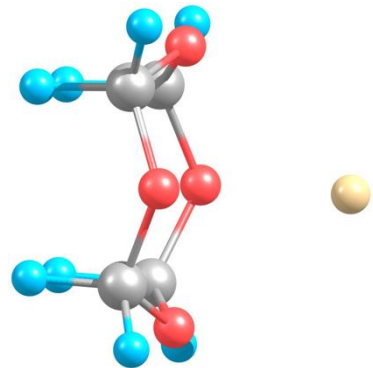


**Figure 2.4.9.** Tetraoxane - Li<sup>+</sup>(Flipped)

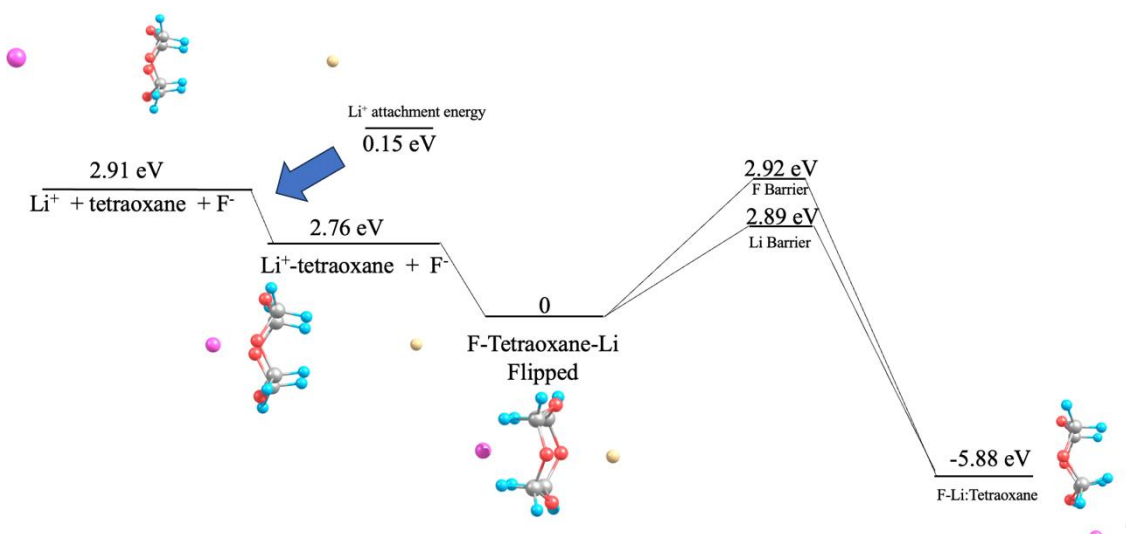


**Figure 2.4.10.** Flipped Tetraoxane Complex Energy Diagram.

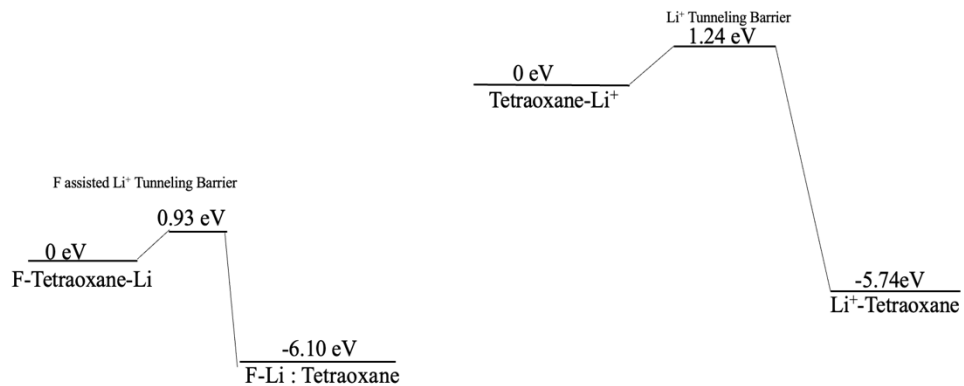


**Figure 2.4.11.**  $\text{Li}^+$  Penetrating Flipped Tetraoxane Energy Barriers

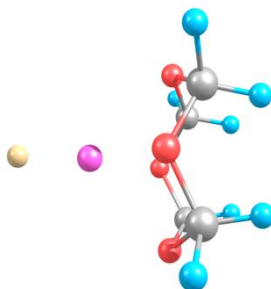
Free Li-F has a dipole moment of 6.5 D and a distance between ions of 1.6 Å (Table 2.2). Tetraoxane has a dipole moment of 3.64 D; LiF traps Tetraoxane in the Li-Tetraoxane-F conformation leading to a dipole moment of 6.94 D, with a Li-F distance of 4.06 Å. Compared to a similar analogous system, Trioxane has a dipole moment of 2.2 D<sup>18</sup>. In the Na-Trioxane-Cl complex, Na-Cl's bond length is stretched from 2.38 Å to 5.26 Å, increasing the dipole moment from 9.25 D (Free Na-Cl) to 15.9 D (Na-Trioxane-Cl)<sup>18</sup>. In the Na-Trioxane-I complex Na-I's bond length of 2.73 Å is stretched to 5.69 Å, increasing the dipole moment from 9.46 D (Free Na-I) to 17.7 D (Na-Trioxane-I)<sup>18</sup>. Here, we can see that in complexation, the dipole moment rises dramatically. The larger dipole moment of Tetraoxane compared to trioxane can explain why the increases in the dipole moment of complexes are larger for Trioxane; this is due to Tetraoxane's larger dipole inside dipole effect counteracting the dipole moment of the stretched ion-pair. In addition, the M-O and X-H distances are significantly shorter in Tetraoxane (2.02 Å/1.88 Å) compared to that in Trioxane (2.2 Å/ 2.26 Å), and this more tightly held tetraoxane system helps explain why the dipole moment of Li-Tetraoxane-F is smaller than that in other comparisons to less polar molecules, such as Trioxane.

With such a significant increase in the distance between Li and F ions in Li-Tetraoxane-F, one might expect the dipole moment to increase significantly to match it, but this expectation is not observed. This effect can be seen when we look at the cis-BzO<sub>3</sub><sup>17</sup> system; the smallest ion pair studied was Na-Cl (9.25 D), and complexation to Na-(cis-BzO<sub>3</sub>)-Cl (12.4 D) had only approximately 34% increase of dipole moment, even when the bond length of Na-Cl (2.38 Å) is stretched to 5.24 Å in Na-(cis-BzO<sub>3</sub>)-Cl<sup>17</sup>. This is due to the dipole-in-dipole effect, the inner dipole moment of tetraoxane countering the ion-pairs dipole moment.

F-Li-Tetraoxane (Figure 2.4.12) and Tetraoxane-F-Li (Figure 2.4.5) have very similar dipole moments at 11.56 D, and 11.61 D respectively. The difference between the two could be due to the larger Li<sup>+</sup> attachment energy compared with F<sup>-</sup>. This explanation is also observed by the increased Li-F distance in F-Li-Tetraoxane of 1.62 Å, compared to 1.60 Å in Tetraoxane-F-Li. Li is more closely held by tetraoxane with a Li-O distance of 2.19 Å compared to the F-H distance of 2.35 Å. The attached

complexes are more polar by approximately 4.5 D (Table 2.2). This relationship is reversed from the M-Trioxane-X cases, where a decrease in the dipole moment of 3-6 D<sup>18</sup> was observed for the side-attached systems compared to the trapped systems.

**Figure 2.4.12** F-Li-Tetraoxane. Li This reversed relationship could be due to the increased polarity of tetraoxane, which is evident in the more polar C<sub>6</sub>H<sub>6</sub>F<sub>6</sub> system having a higher dipole moment in the Mol-XM compared to M-C<sub>6</sub>H<sub>6</sub>F<sub>6</sub>-X by 1.4 D<sup>16</sup>. This trend is also found in X-M-(cis-BzO<sub>3</sub>) and (cis-BzO<sub>3</sub>)-X-M systems, where side attached conformation has a larger dipole moment than the trapped M-(cis-BzO<sub>3</sub>)-X<sup>17</sup>.



The calculated IR intensity spectrum of tetraoxane (Figure 2.4.14) contains two groups of peaks of large intensity, at  $1200\text{ cm}^{-1}$  and  $3000\text{ cm}^{-1}$ .

The peak groups at  $1200\text{ cm}^{-1}$  contain the brightest peak, due to vibrations of the C-O bonds in the  $\text{C}_4\text{O}_4$  ring and the rocking motions of the  $\text{CH}_2$ . The peak at  $3000\text{ cm}^{-1}$  is due to axial C-H stretching. In comparison to trioxane<sup>18</sup>, the peaks are very similar to differences in the  $1200\text{ cm}^{-1}$  area, whereas the tetraoxane peaks are more intense. The peaks at  $1200\text{ cm}^{-1}$  are twice as intense as the peaks at  $3000\text{ cm}^{-1}$ , whereas in trioxane, the ratio is 3:2 for lower to higher frequencies.

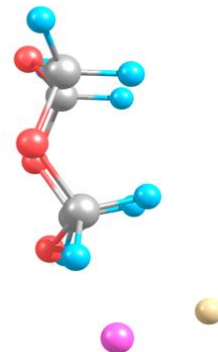


**Figure 2.4.13.** Tetraoxane side attached.

#### 2.4.1.1 Tetraoxane Infrared Spectra

In the IR spectra for the complex Li-Tetraoxane-F (Figure 2.4.14), the peak at  $3000\text{ cm}^{-1}$  splits into two peaks. This corresponds to the stretching of the four inner  $\text{CH}_2$  groups that point towards the fluorine atom. This peak band maintains its overall intensity but has two peaks contributing, this could be due to the  $\text{CH}_2$  group oriented along the axis (pointing towards fluorine). Those pointing away radially, leading to the formation of two peaks,

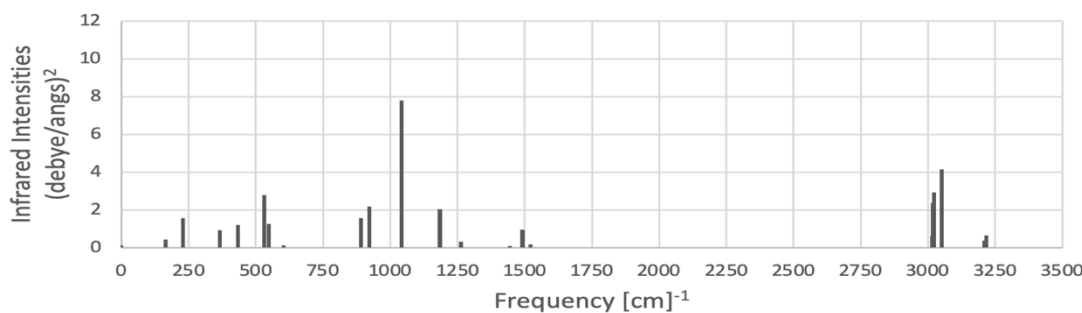


**Figure 2.4.14.** IR Spectra of Li-Tetraoxane-F.  
have the compression of the molecule by the ion pair and can help to explain the shift in the peaks. The peak at  $3000\text{ cm}^{-1}$  is the second brightest peak in the predicted spectra. The brightest peak is at  $1040\text{ cm}^{-1}$ , this peak is red-shifted from the  $1200\text{ cm}^{-1}$  peak in isolated

tetraoxane. This peak is the result of vibrations of the  $C_4O_4$  ring and, the rocking motions of the  $CH_2$  groups as well. Many notable peaks are red-shifted , with only one smaller peak showing a blue shift at  $1500\text{ cm}^{-1}$ .

When Li-F settles on the side of tetraoxane in the Li-F: Tetraoxane geometry (Figure 2.4.13), distinctive changes are observed (Figure 2.4.16). The brightest peak is located at  $1210\text{ cm}^{-1}$ , and this peak is very similar to the most intense peak for the isolated tetraoxane system. The biggest difference from the isolated tetraoxane is in the peak around  $3000\text{ cm}^{-1}$ : in the side attached system, the peak is significantly suppressed to a third of its original value and retains its doublet nature found in the trapped geometry. This peak suppression is due to the fluorine pulling on the hydrogen and holding it tighter, suppressing C-H stretches.

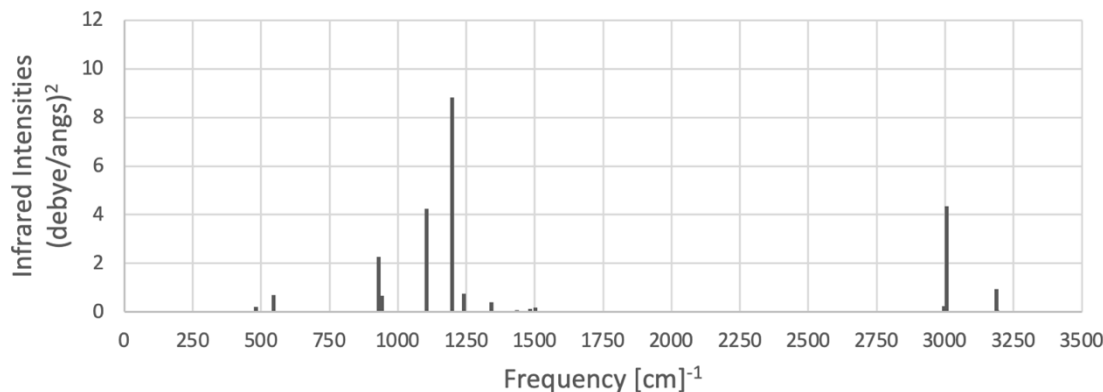


**Figure 2.4.15.** Infrared Spectra of Tetraoxane isolated.

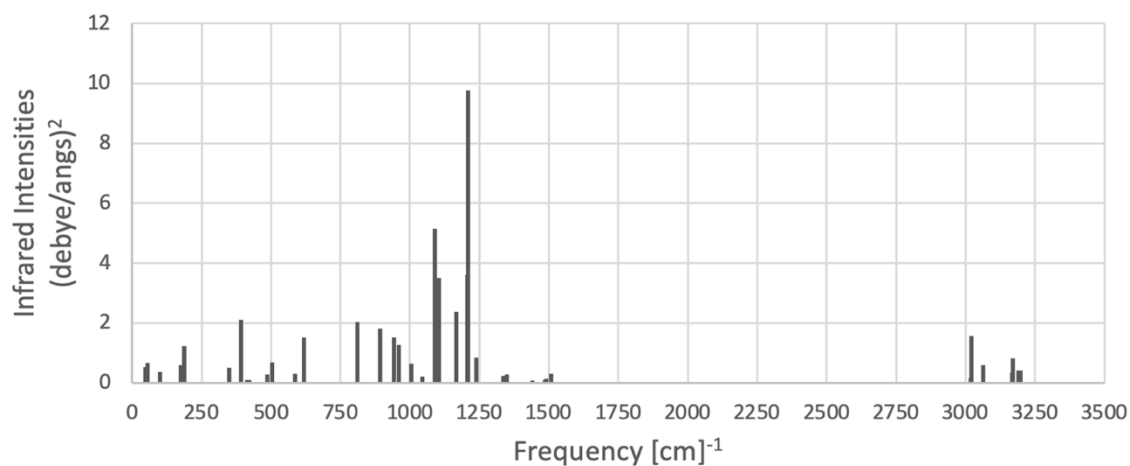


**Figure 2.4.16.** Infrared Spectra of Li-F:Tetraoxane (side attached).

A comparison of the three geometries of tetraoxane mentioned above; isolated, trapped and side attached geometry (Figure 2.4.17). We can see these peak shifts, mostly the red shifting of the peak around  $1100\text{ cm}^{-1}$ , this shift is the largest in the trapped geometry and shows mild shifting in the side attached geometry. Interestingly, the peak at  $1200\text{ cm}^{-1}$  is strong in both the isolated and side-attached geometries. The trapped

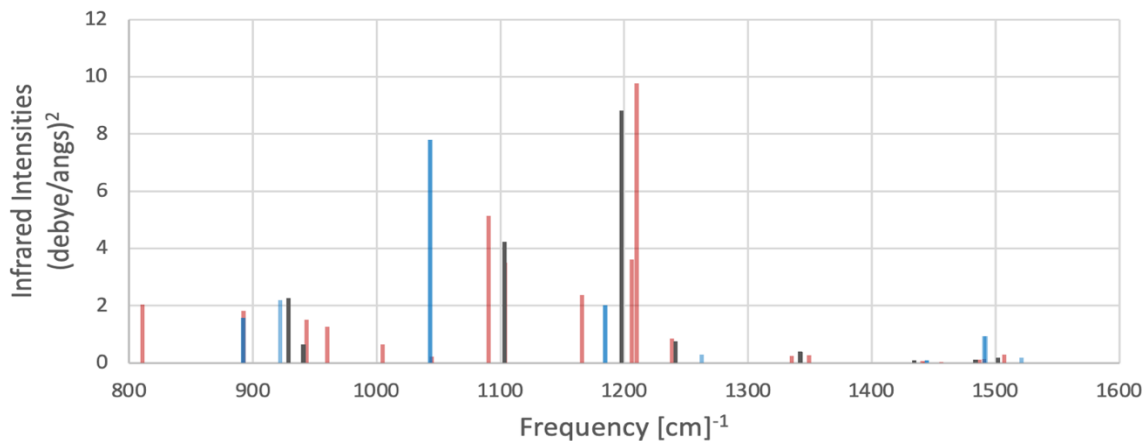


**Figure 2.4.17.** Infrared Spectra of Tetraoxane combined. Red-side attached, blue-trapped, black-isolated).

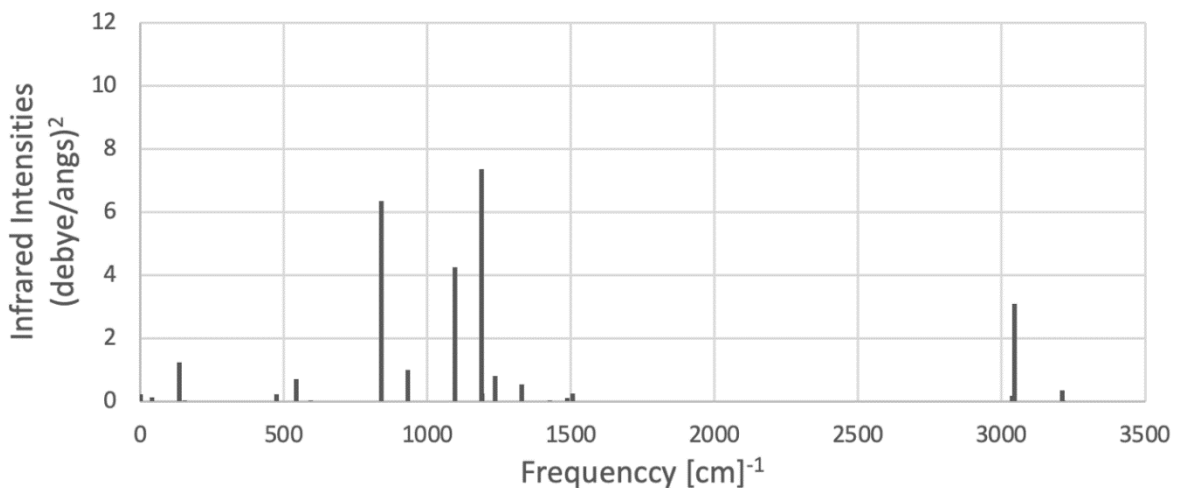


**Figure 2.4.18.** Infrared Spectra of F-Li-Tetraoxane (Li point).

geometry significantly suppresses this  $1200\text{ cm}^{-1}$  peak, which could be due to the molecule being held tightly between the Li-F counterions, hindering its vibrations.

Ion-pair attachment was also studied using computed IR spectra for tetraoxane, where the ion pair can attach to either side. These two systems are when Lithium points toward the oxygen side (Figure 2.4.18) and fluorine pointing towards the C-H side (Figure 2.4.19). Interesting information comes from these two figures that can support the interpretation of the peak at  $3000\text{ cm}^{-1}$  being from the C-H axial group, as Tetraoxane-F-Li has the largest suppression to this peak compared to that of isolated Tetraoxane. This peak suppression is due to the fluorine pulling on the hydrogen and holding it tighter, suppressing their stretches.

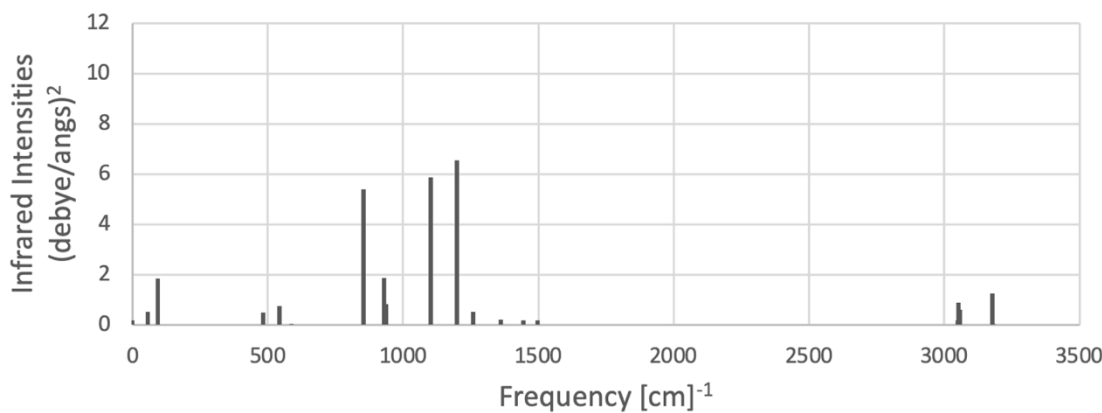


**Figure 2.4.19.** Infrared Spectra of Tetraoxane-F-Li (F point).

## 2.4.2 Pentaoxecane

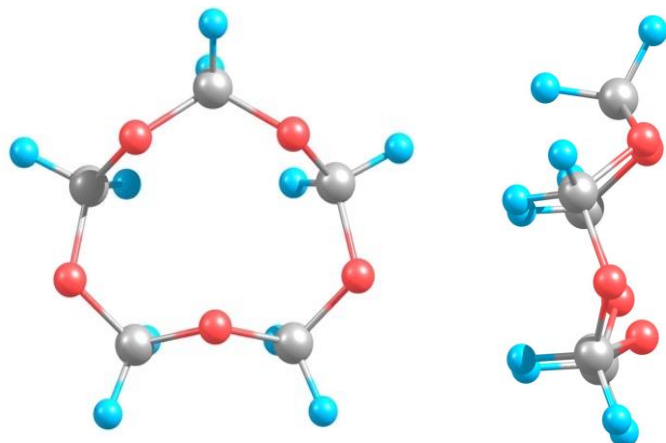


**Figure 2.4.20.** Pentaoxecane front view (Left), side view (Right).

Pentaoxecane (Figure 2.4.20) is a medium-sized organic cyclic molecule that can be inserted and noncovalently trapped between alkali-halide counter ions, such as Li-F. Pentaoxecane is a crown-type cyclic system  $C_5O_5H_{10}$ , alternating  $CH_2$  and oxygen groups. This system is polar, similar to that of previously described tetraoxane; this system

has a similar folding ability to cyclooctane and other larger cyclic molecules. This folding ability is seen in the hydrogen atom at the top of [Figure 2.4.20 (right) and Figure 2.4.21 (right)] bending towards lithium in the trapped Li-Pentaoxecane-F. Pentaoxecane is the most polar of the isolated molecules in this study, with an appreciable dipole moment of 4.40 D. This significant dipole moment is due to the electronegativity of the oxygen atoms in the molecule, which pulls electron density towards them. The oxygen side of pentaoxecane is negative, and the hydrogen side is positive in charge. This polar property of Pentaoxecane facilitates the attachment of ion pairs, lithium toward the oxygen side and fluorine toward the hydrogen side.

$\text{Li}^+$ -Pentaoxecane (Figure 2.4.22.) system has a significant attachment energy for  $\text{Li}^+$ , 3.86 eV, which is the second largest of the systems studied here ( $\text{Li}^+$ -Tetraoxane being greatest). In addition to being the second-highest ion attachment studied, it is also significantly larger than previously studied analogous systems such as  $(\text{Cs}^+)$ -Trioxane. In the  $(\text{Cs}^+)$ -Trioxane system ion attachment is 0.97 eV<sup>18</sup>, in  $(\text{Cs}^+)$ -BzO<sub>3</sub> ion attachment is 1.58 eV<sup>17</sup>, and

in the polar  $\text{Cs}^+$ -C<sub>6</sub>H<sub>6</sub>F<sub>6</sub> ion attachment is limited to 1.24 eV<sup>16</sup>. This considerable attachment energy promotes the formation of the insertion complex by the possible pathway of having a  $\text{Li}^+$  ion coordinate first quite favorably before F<sup>-</sup> ion coordinates to the opposite side.

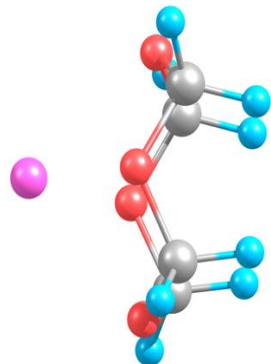


**Figure 2.4.22.**  $\text{Li}^+$ -Pentaoxecane.

In Pentaoxecane-F<sup>-</sup> (Figure 2.4.23.) F<sup>-</sup> has an attachment energy of 1.76 eV, larger than the tetraoxane system. F<sup>-</sup> having a lower attachment energy supports the previously stated pathway of  $\text{Li}^+$  attaching first followed by F<sup>-</sup>. Ion attachment in M-Trioxane-X also has an I<sup>-</sup> attachment to the mol lower than the Cs<sup>+</sup>, 0.68 eV compared to 0.97 eV<sup>18</sup> respectively. This reduced F<sup>-</sup> attachment energy is due to the (Li<sup>+</sup>) proximity to the oxygens, compared to fluorine's proximity to the hydrogens.

Once the complex is formed, energy barriers keep it together, this is shown in the energy diagram (Figure 2.4.24). An energy barrier of 2.24 eV was found for lithium to travel around the molecule. No energy barrier for F<sup>-</sup> to travel around the ring was able to be found. Li-Pentaoxecane-F complex has a D<sub>e</sub> of 1.12 eV relative to Li-F+Pentoxecane, holding the complex together.

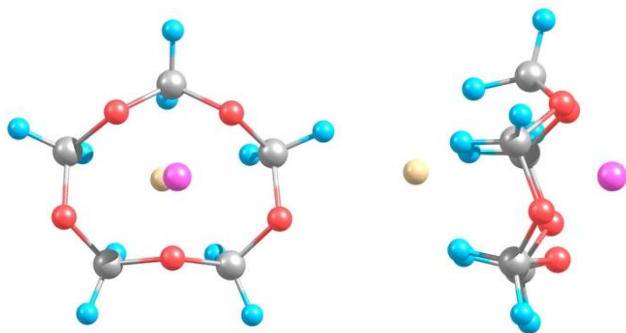


**Figure 2.4.21.** Li-Pentaoxecane-F front view (Left), Side view (Right).

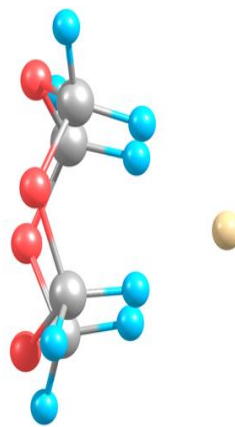


**Figure 2.4.23.** Pentaoxecane- $F^-$

Two Lithium energy barriers were studied, one for penetrating and one for recollection with Florene around the side of the system. Pentaoxecane is most interesting for its lithium penetrating effects (Figure 2.4.25); once complexation has occurred, the energy barrier for Lithium to penetrate through the molecule is only 0.48eV, which is the lowest energy barrier of the systems studied. It is also noteworthy that the energy for Li is much lower to penetrate than to move around the molecule. Pentaoxecane opens up slightly when the Li- Pentaoxecane -F complex is formed from a gap area of  $8.61\text{ \AA}^2$  in Pentaoxecane to  $8.72\text{ \AA}^2$  in the complex. We calculated the gap area by determining the area between the five oxygen atoms of the cyclic molecule and the three smaller triangles that form a pentagon. The size of the gap is also measured by the min and max distance of opposed carbons,  $3.79\text{ \AA}$  (free complex) to  $3.89\text{ \AA}$  (inserted complex) and  $3.81\text{\AA}$  (free complex) to  $4.11\text{\AA}$  (inserted complex). This opening is interesting because it can assist in the penetrating of  $\text{Li}^+$  through the molecule by reducing the steric effects of  $\text{Li}^+$  passing through.

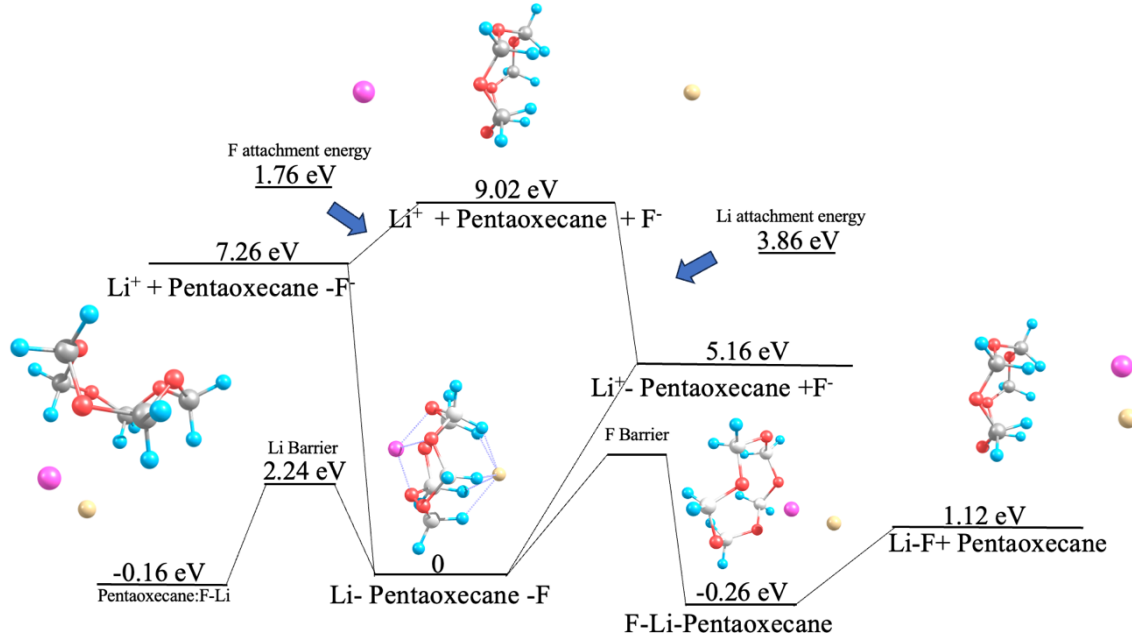


**Figure 2.4.24** Pentaoxecane Complex Energy Diagram .

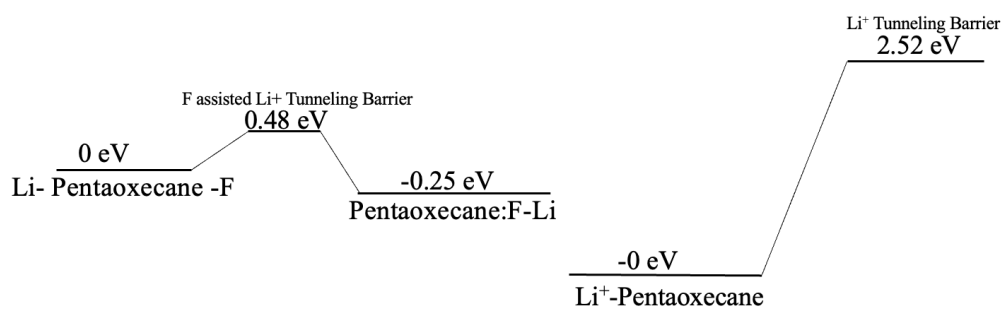
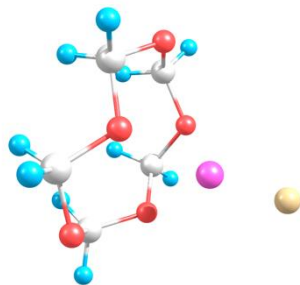


**Figure 2.4.25**  $\text{Li}^+$  Penetrating Pentaoxecane Energy Barriers.

Pentaoxecane is a polar cyclic molecule with the largest dipole of the three systems studied at 4.40 D (Table 2.2). The  $\text{Li}$ -Pentaoxecane-F complex has a  $\text{Li}$ -F distance of 3.72 Å and a dipole moment of only 4.36D. This ion-pair bond length is the shortest distance in a trapped conformation found in this study. Interestingly, the dipole moment is smaller than that of the overall dipole moment of ether free pentaoxecane (4.40 D) or  $\text{Li}$ -F (6.5 D). Here, the dipole inside dipole effect is profound, counteracting a large portion of the dipole moment due to the stretch of  $\text{Li}$ -F from 1.6 Å to 3.72 Å. Even with the more polar  $\text{C}_6\text{H}_6\text{F}_6$  (6.2 D)<sup>26</sup>,  $\text{M-C}_6\text{H}_6\text{F}_6\text{-X}$  ( $\text{M-X} = \text{Cs-I}, \text{Cs-Cl}$ ) systems were found to have significantly larger dipole moments by approximately double than free  $\text{M-X}$ . This interesting property is most likely due to the large size of the cyclic molecule, which allows the ion pair to sit deeply inside Pentoxecane. This is because of two factors, the first being that the molecule is larger compared to tetraoxane or trioxane, letting the ion pair sit more deeply inside the cyclic molecule. The second is the larger dipole moment of Pentaoxecane pulling the Ion pair more strongly towards it reducing the  $\text{Li}$ -F stretched distance in the complex, and the larger the dipole moment of mol than the stronger the DID effect reducing the overall dipole moment of the complex.

In an earlier study of  $\text{C}_6\text{H}_6\text{F}_6$ , trapped  $\text{Cs}-\text{C}_6\text{H}_6\text{F}_6-\text{I}$  has a  $D_e$  0.91 eV relative to  $\text{Cs}-\text{I} + \text{C}_6\text{H}_6\text{F}_6$ , with energy barriers of 0.8–1 eV of recollection around the molecule<sup>16</sup>. The  $\text{Re}$  of  $\text{Cs}-\text{I}$  bond length is stretched by twice in the  $\text{Cs}-\text{C}_6\text{H}_6\text{F}_6-\text{I}$  complex. The dipole moment is increased to 20D in the trapped complex compared to 12.3D in free  $\text{Cs}-\text{I}$ .  $\text{C}_6\text{H}_6\text{F}_6$  has a dipole moment of 6D, which is relatively high and larger than Pentaoxecane. It is of note that the Li-Pentaoxecane-F complex has a dipole moment that is not larger than parts. In contrast, these previously studied systems have a significantly larger dipole moment in complexation.

$\text{F-Li-Pentaoxecane}$  (Figure 2.4.26) has a significant dipole moment of 12.31D, which value is similar to the other polar systems of  $\text{F-Li-Tetraoxane}$  (11.56D) and  $\text{Tetraoxane-F-Li}$  (11.61D). The side-attached complex is more polar (Figure 2.4.27) than the trapped complex for pentaoxecane, by 8 D. This is the most significant increase in the dipole moment of a side-attached XM-Mol or Mol-XM compared to an M-Mol-



X system discovered in this study. This increased dipole moment of the side attached follows the trend that with a larger dipole moment of Mol, the side attached XM-Mol's dipole moment will also be larger, similar to the  $\text{C}_6\text{H}_6\text{F}_6^{18}$ ,

**Figure 2.4.26.**  $\text{F-Li-Pentaoxecane}$  "Li Point". cis- $\text{BzO}_3^{17}$  and tetraoxane cases.

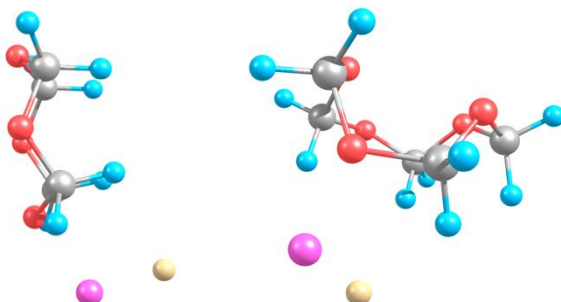


**Figure 2.4.27.** Pentaoxecane:Li-F side attached.

#### 2.4.2.1 Pentaoxecane Infrared Spectra

The calculated IR intensity spectrum of Pentaoxecane (Figure 2.4.28-2.4.30) exhibits two major groups of peaks, near  $1200\text{ cm}^{-1}$  and  $3000\text{ cm}^{-1}$ . The peaks around  $1200\text{ cm}^{-1}$  are the brighter of the two groups and are due to the vibrations of the C-O molecule as well as the rocking motions of the  $\text{CH}_2$  groups. The group around  $3000\text{ cm}^{-1}$  corresponds with axial C-H stretches. For comparison trioxane previously studied <sup>18</sup>, also has peaks around  $1200\text{ cm}^{-1}$  and  $3000\text{ cm}^{-1}$ . The apparent difference is around  $3000\text{ cm}^{-1}$ , where Pentaoxecane has many less intense peaks than trioxane's bright peak at  $3000\text{ cm}^{-1}$ . This difference is due to the increased number of C-O bonds that vibrate and its slightly bent cyclic molecule shape, making each C-O group different from the others. Compared to Tetraoxane, Pentaoxecane also has significantly more peaks in the  $3000\text{cm}^{-1}$ . This increase in number of peaks in the  $3000\text{cm}^{-1}$  range is also due to the increased number of C-O bonds, and the bent nature of the Pentaoxecane.

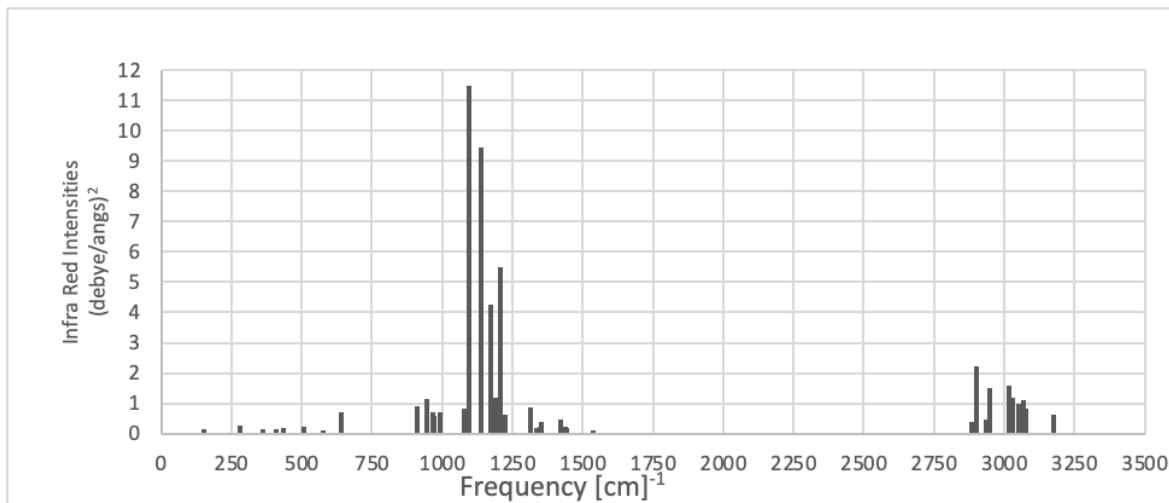


**Figure 2.4.28.** Infrared Spectra of Pentaoxecane.

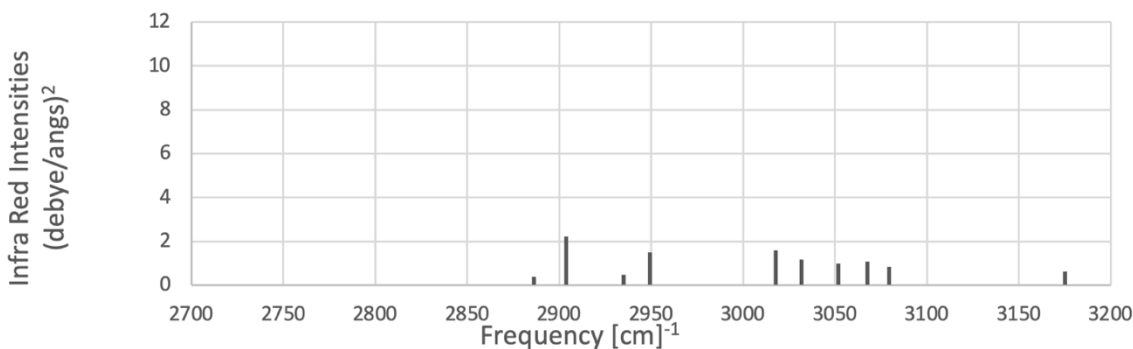


**Figure 2.4.29.** Infrared Spectra of Pentaoxecane. Range  $2700\text{ cm}^{-1}$ - $3200\text{ cm}^{-1}$ .

In the insertion complex Li-Pentaoxecane-F (Figure 2.4.31-2.4.33), the peaks from the  $1200\text{ cm}^{-1}$  area are slightly red-shifted closer to  $1000\text{ cm}^{-1}$ . This red shifting could result from an increase in the bond length of the C-O bond in the complex(C-O bond length of  $1.41\text{ \AA}$  in Pentaoxecane and  $1.44\text{ \AA}$  in Li-Pentaoxecane-F). The peak group around  $3000\text{ cm}^{-1}$  is blue-shifted, and all peaks now are above  $3000\text{ cm}^{-1}$ . This peak blue shift is likely due to the ion pair (Li-F) squeezing the system, increasing the vibrational frequency. This group also becomes more tightly packed, which might result from the ion pair's flattening

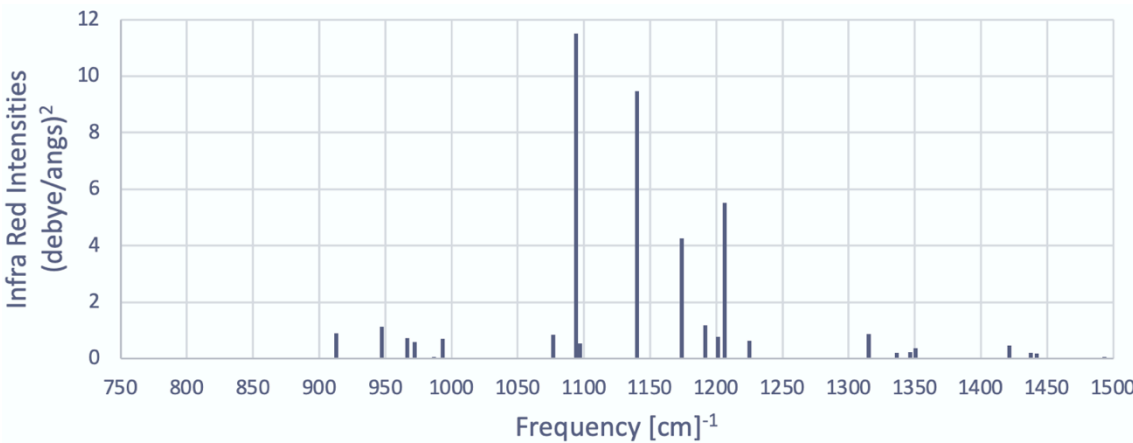


**Figure 2.4.30.** Infrared Spectra of Pentaoxecane. Range  $750\text{ cm}^{-1}$ - $1500\text{ cm}^{-1}$ .

effect on the molecule. The flatter systems become more symmetrical because each C-O bond becomes more similar to each other, reducing the spread of peaks. Compared to the trioxane case, we see an increase in the peaks around the  $3000\text{ cm}^{-1}$  area, but to a lesser extent. Compared to Tetraoxane, there is an increase in the number of peaks in the higher frequency range (around  $3000\text{cm}^{-1}$ ). One clearer indication of the difference between Li-

Pentaoxecane-F and Li-Tetraoxane-F is the peak at  $3200\text{cm}^{-1}$ . Which in the Pentaoxecane system is significantly suppressed compared with that of the tetraoxane complex.

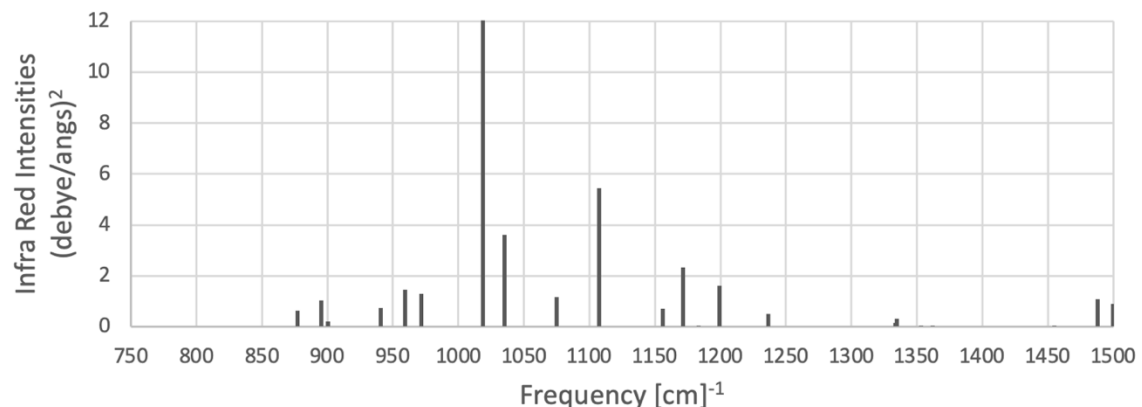


**Figure 2.4.33.** Infrared Spectra of Li-Pentaoxecane-F. Range  $750\text{ cm}^{-1}$ - $1500\text{ cm}^{-1}$ .

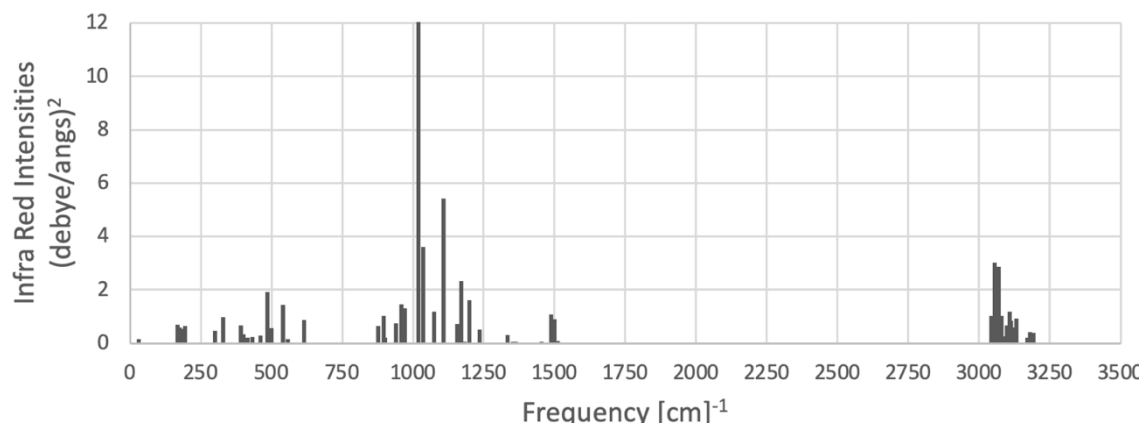


**Figure 2.4.31.** Infrared Spectra of Li-Pentaoxecane-F.

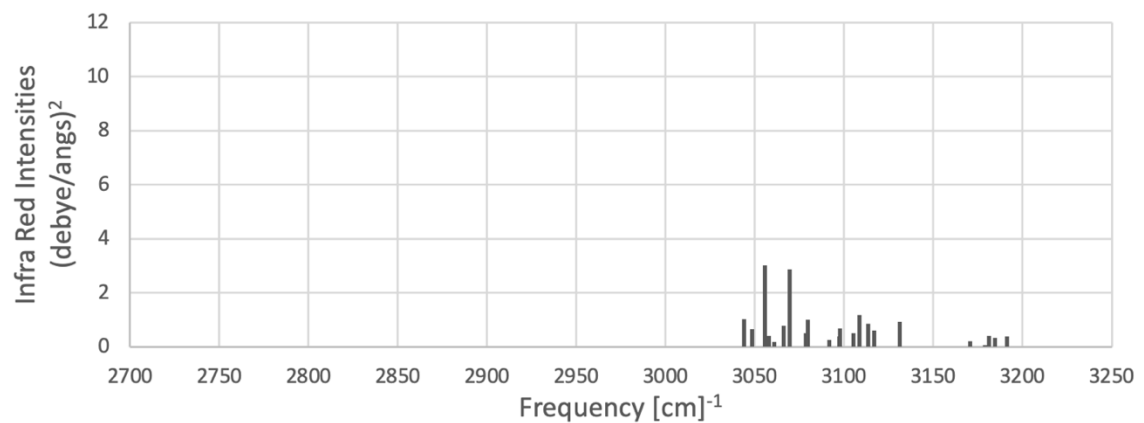


**Figure 2.4.32.** Infrared Spectra of Li-Pentaoxecane-F. Range  $2700 \text{ cm}^{-1}$ - $3200 \text{ cm}^{-1}$ .

### 2.4.3 Cyclooctane

Cyclooctane is a cyclic molecule with eight CH<sub>2</sub> groups (Figure 2.4.34) and has a slight fold in its structure (Figure 2.4.34 right). This system is not polar, unlike Tetraoxane and Pentaoxecane, with a lack of charge-dipole attraction reducing the ability to stabilize the complex. This non-polar nature leads to the Li-

Cyclooctane-F complex (Figure 2.4.35) having a D<sub>e</sub> of -2.04 eV relative to Cyclooctane+Li-F. A negative dissociation energy indicates that the system is metastable, being higher in energy than its parts, and held together by energy barriers. Complexation stretches the Li-F bond to 4.16 Å. This bond stretch without an inner opposed dipole created the second largest dipole moment in this study of 10.74 D (F-Tetraoxane-Li flipped being the largest). Li<sup>+</sup> attachment energy to cyclooctane is 1.46 eV; this is the second lowest value for the three systems studied (again Flipped Tetraoxane-Li<sup>+</sup> is smaller). It is interesting to note that after penetration or recollection around cyclooctane, the side attached F-Li:Cyclooctane (Figure 2.4.36) is recovered. No point system was found to be stable, point system being when the one side of the ion pair is attached to a face of the cyclic molecule with the other

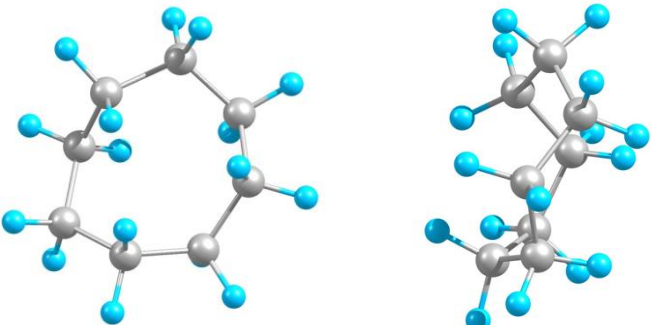


**Figure 2.4.34.** Cyclooctane front view(Left), Side view (Right).

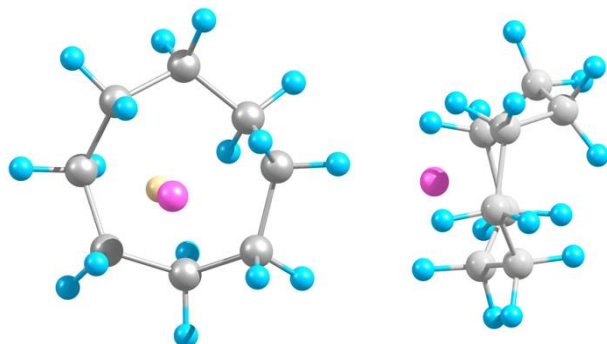


**Figure 2.4.35.** Li-Cyclooctane-F. Front View (Left), Sideview (Right).

pointing away such as in the F-Li-Pentaoxecane Li point system (Figure 2.4.26) . F-Li:Cyclooctane is equivalent to Cyclooctane:F-Li in that Li-F placed on either side recovers to the same side-attached conformer.

After forming the Li-Cyclooctane-F complex, energy barriers keep the system together; four barriers are studied here (Figure 2.4.37, 2.4.38). They are for lithium moving around the molecule, lithium penetrating assisted by fluorine,  $\text{Li}^+$  penetrating unassisted, and  $\text{F}^-$  moving around the molecule. Lithium moving around the molecule in the complex is the minor energy barrier at 0.24 eV in height; after lithium moves around, it recollects with fluorine onto the side of Cyclooctane into the Cyclooctane:F-Li conformation. The energy barrier for lithium penetrating the complex was 0.32 eV; the  $\text{F}^-$  counter ion assists this. After penetration, the side attached Cyclooctane:F-Li is recovered. The energy barrier for fluorine moving around the molecule towards lithium is 0.42 eV; after the ions have recollected, the side-attached conformation is recovered. The energy barrier for  $\text{Li}^+$  ion unassisted penetrating the molecule is 0.67 eV, the highest energy barrier for cyclooctane. These values are similar to energy barriers found for the analogous system Li-Cubane-F and Li-ladderene-F. Li-Cubane-F has energy barriers for recollection of ions around cubane of 0.4 eV and 0.35 eV

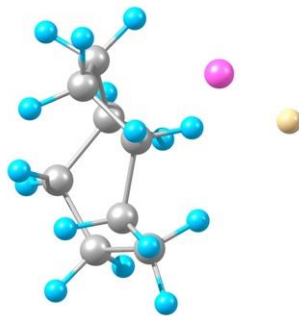


**Figure 2.4.36.** Cyclooctane:Li-F.

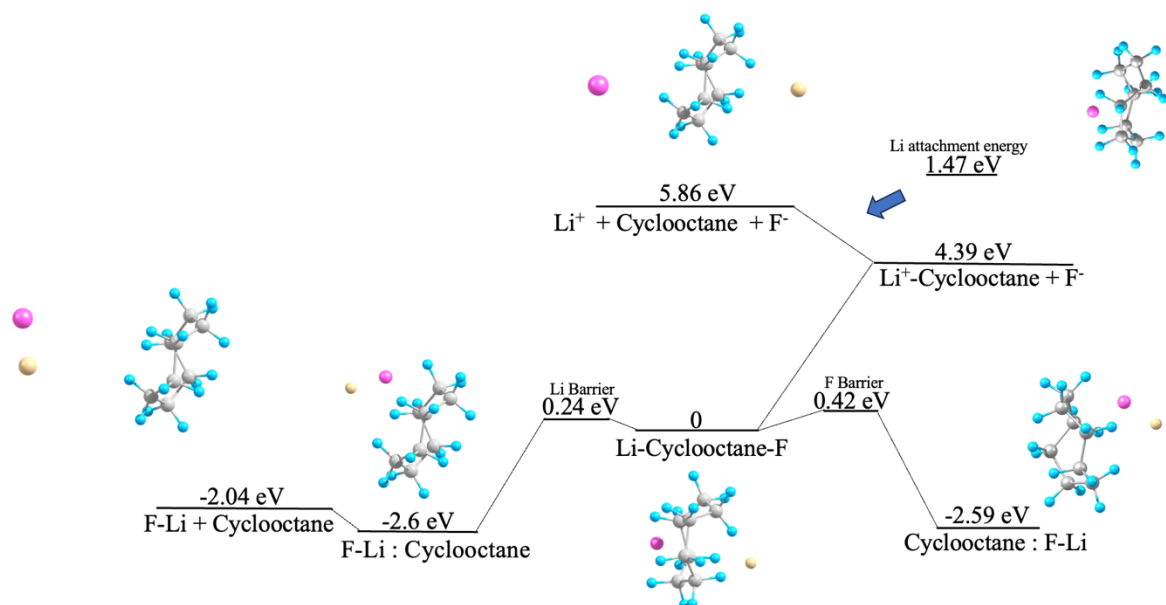


**Figure 2.4.37.** Cyclooctane Complex Energy Diagram.

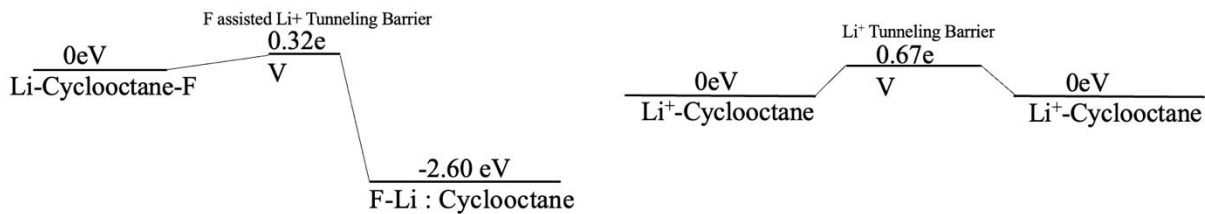


**Figure 2.4.38**  $\text{Li}^+$  Penetrating Cyclooctane Energy Barriers.

for lithium and fluorine, respectively <sup>12</sup>. Li-ladderene-F has smaller energy barriers for recollection of  $0.1\text{ eV}$  and  $0.15\text{ eV}$  <sup>12</sup>. Therefore, Li-F can trap cyclooctane more effectively than ladderene and approximately as well as cubane.

In  $(\text{Li}^+)$ -Cyclooctane, the molecule generally preserves its geometry compared to the trapped complex, with  $\text{Li}^+$  ion slightly farther away from the molecule (Table 2.2). This increase in distance is due to the missing  $\text{F}^-$  counterion on the other side.  $\text{Li}^+$  attachment energy of  $1.46\text{ eV}$  is higher than that in analogous systems, such as  $0.83\text{ eV}$  in  $\text{Li}^+$ -cyclohexane<sup>16</sup>,  $0.92\text{eV}$  in  $\text{Li}^+$ -adamantane <sup>24</sup>, and  $1.09\text{eV}$  in  $\text{Li}^+$ -cubane<sup>12</sup>. Its attachment energy is slightly less than that of  $1.5\text{eV}$  in  $\text{Li}^+$ -Ladderene <sup>12</sup>. This increase in attachment energy could be due to the molecule's increased size, allowing  $\text{Li}^+$  to sit more deeply inside the cyclic molecule, closer to the slightly negatively charged carbons and farther from the slightly positively charged hydrogens. This is shown by  $\text{Li}^+$  having a distance to the closest hydrogens of the molecule of  $2.1\text{\AA}$  in  $\text{Li}^+$ -Cyclooctane. In ladderene  $\text{Li}^+$  sits closer to more carbons than in cubane and has higher attachment energy because of this increased distance to hydrogens and reduced distance to carbons <sup>12</sup>.

$\text{Li-Cyclooctane-F}$ 's negative  $D_e$  indicates it is metastable. As stated previously this is due to cyclooctane being non-polar, having no dipole moment to help attract the ions. This trend is seen in analogous nonpolar systems. Such as  $\text{Li-Cubane-F}$  and  $\text{Li-Lad-F}$  both have negative dissociation energies,  $-2.93\text{eV}$  and  $-2.5\text{eV}$  respectively

<sup>12</sup>. Interestingly, the Li-Cyclooctane-F  $D_e$  value of -2.03eV is significantly lower than that of analogous systems; this could be due to the larger size of the molecule, allowing the ion pair to be more deeply set, lowering the distance bond length of the ion pair and increasing stability. Indeed, this is the case because the distance between ions in Li-cyclooctane-F is 4.38 Å (Table 2). This distance is lower than in analogous systems and can add to the stability of the system and a reduction in dipole moment. Li-Cubane-F distance is 5.59 Å, and Li-Ladderene-F is 5.25 Å <sup>12</sup>, both significantly larger than Li-Cyclooctane-F. Li-C<sub>4</sub>H<sub>8</sub>-Cl has an M-X distance of 4.71 Å <sup>13</sup>, indicating that smaller cyclic molecules increase the M-X distance.

Both F-Li:Cyclooctane and Cyclooctane:F-Li side attached systems were studied, but both resulted in similar conformation with LiF settling on the side of cyclooctane; they have dipole moments of 6.06 D and 6.08 D, respectively. This recovery to the same geometry is interesting because Cyclooctane is not symmetrical, having a slightly folded structure, as seen in (Figure 2.4.34. Right). Side attached Li-F in Li-F:Cyclooctane forces an inversion of the cyclic molecule with F slightly repelling from the molecule. In forming this side attached conformer, 0.5 D of dipole moment is lost due to the small amount of charge donated to the molecule in this orientation.

The smaller hydrocarbon cyclic molecule C<sub>6</sub>H<sub>12</sub> was previously studied with Cs-I as the trapping ion pair and has a dipole moment of 25D <sup>16</sup>. This large dipole moment of Cs-C<sub>6</sub>H<sub>12</sub>-I complex is larger than those for the polar system Cs-C<sub>6</sub>F<sub>6</sub>-I (20 D), this is due to no internal dipole competing with the stretched ion-pair dipole moment. Cs-C<sub>6</sub>H<sub>12</sub>-I large dipole moment is significantly larger than the values for cyclooctane found in this study.

In addition, Cs-C<sub>6</sub>H<sub>12</sub>-I has a negative value for  $D_e$  at -1.2eV <sup>16</sup> compared to Cs-I + C<sub>6</sub>H<sub>12</sub>; the negative value for complexation is similar to that of Li-cyclooctane-F complex (-2.04 eV) because of no stabilization effect from the molecule because of its lack of polarity. In the Cs-C<sub>6</sub>H<sub>12</sub>-I system, Cs-I does not sit in the center of the molecule

but somewhat off to the side. This off-center positioning corresponds to an energy barrier of  $\text{Cs}^+$  ion's recollecting of 0.2eV, which is similar to that of the  $\text{Li}^+$  recollecting in the Li-Cyclooctane-F system. Naumkin<sup>16</sup> reports  $\text{I}^-$  ions energy barrier for recollection of 0.3 eV in the  $\text{Cs-C}_6\text{H}_{12}\text{-I}$  system, this is larger than the  $\text{F}^-$  ion energy barrier for Li-Cyclooctane-F. The increased energy barrier for  $\text{I}^-$  vs  $\text{F}^-$  ion recollection around these similar cyclic hydrocarbons could be due to  $\text{F}^-$ 's size being smaller and more mobile. In  $\text{Cs-C}_6\text{H}_{12}\text{-I}$  the ion's off-axis attachment is interesting because the ions in trapped Li-Cyclooctane-F sit more deeply inside the molecule than in  $\text{Cs-C}_6\text{H}_{12}\text{-I}$ . This can be explained by the difference in size of the counter ions, the lithium energy barrier for recollecting around the molecule is half the energy of fluorine's energy barrier. Lithium is known for its mobility and is often selected for this property.

Two  $\text{C}_8\text{H}_8$  isomers, cubane and 3-ladderene, are non-polar systems studied with  $\text{Li-F}$  as counter ions to trap and form complexes<sup>12</sup>. Li-Cubane-F has a  $D_e$  of -2.93 eV, which is more significant than that of Li-Cyclooctane-F<sup>12</sup>. The Li-F distance in complexation is stretched to 5.59 Å, with a 16.7D dipole moment<sup>12</sup>. Li-(3-laderene)-F has lower energy at a  $D_e$  of -2.5 eV, still metastable; Cyclooctane's larger size lets the ion pair sit more deeply inside. Li-F bond distance in complexation is 5.25 Å with a dipole moment of 16.21 D. Cyclooctane has a lower  $D_e$  energy and a similar energy barrier for Li and F ion recollection. In Li-Cyclooctane-F, the Li-F has a distance between them of  $R_e$  of 4.16 Å; this shorter  $R_e$  distance in analogous cubane and ladderane systems results in a smaller dipole moment.

In the case of  $\text{Li-C}_3\text{H}_6\text{-F}$ , the Li-F distance is 4.35 Å, with a dipole moment of 14.5D<sup>51</sup>. In the case of  $\text{Li-C}_6\text{H}_{12}\text{-F}$ , the Li-F distance is 4.285<sup>24</sup>. For other ion pairs, such as  $\text{Cs-I}$  (12.3 D<sup>1</sup>), we can also see significant increases in dipole moments in trapped conformation, such as in  $\text{Cs-C}_4\text{H}_8\text{-I}$  where the dipole moment is increased to 24.3 D<sup>13</sup>, and  $\text{Cs-C}_6\text{H}_{12}\text{-I}$ , where the dipole moment is increased to 24.6 D<sup>16</sup>. With these comparisons, we can see three main trends. First, as the distance between Li-F increases, the dipole moment also increases, which is consistent with expectation.

Second, we can see that as the cyclic molecule size starts to grow radially, the Li-F distance starts to decrease; this can be explained by the fact that the larger the molecule, the more deeply the ion pair can sit inside, and the molecule offers less steric effect for the ion pair. Third, these ion-trapped non-polar systems have significant dipole moments, as the molecule has no competing internal dipole moment, reducing the overall dipole moment.

#### 2.4.3.1 Cyclooctane Infrared Spectra

The calculated spectra of the infrared intensities (Figures 2.4.39-2.4.41) show the differences and similarities of cyclooctane, Li-Cyclooctane-F complex and side attached systems. Cyclooctane has two significant areas of vibrations, that being  $1500\text{ cm}^{-1}$  and  $3000\text{ cm}^{-1}$ , the latter being much brighter than the former. The brighter  $3000\text{ cm}^{-1}$  dominates this spectrum (Figure 2.4.39) and is due to the C-H stretching of the  $\text{CH}_2$  groups. Interestingly, compared to that of  $\text{C}_6\text{H}_6^{16}$ , the larger breadth of this group is due to the low symmetry of the cyclooctane due to its ring folding. The second group is around  $1500\text{ cm}^{-1}$  due to the other C-H rocking motions. The low-intensity lines around  $750\text{ cm}^{-1}$  are from the C-C stretches of the molecule.

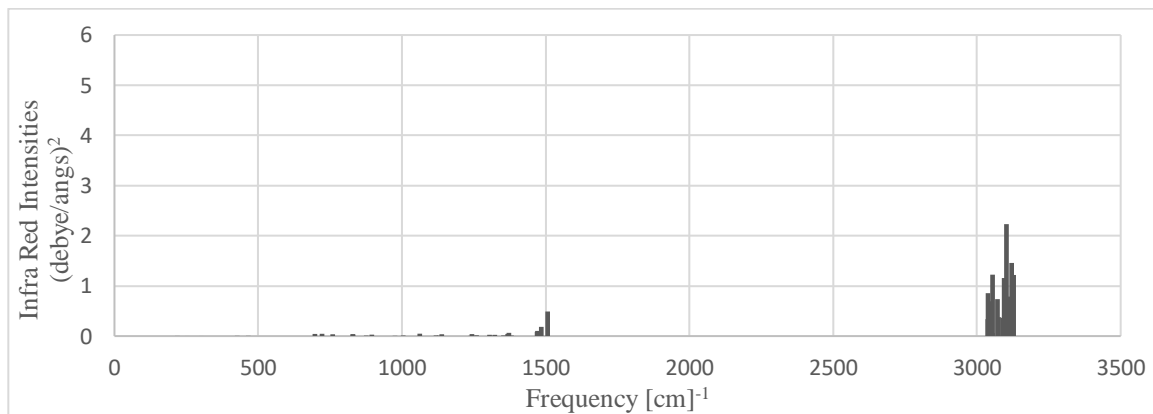


**Figure 2.4.39.** Infrared Spectra of Cyclooctane.

The calculated spectrum for the trapped system Li-Cyclooctane-F (Figure 2.4.40) has significant changes that help identify it from isolated cyclooctane. Firstly, at the  $3000\text{ cm}^{-1}$  area, we have an order of magnitude reduction of the intensity of the signal with a slight red shift of  $200\text{ cm}^{-1}$  from just over  $3000\text{ cm}^{-1}$  in isolated to just under  $3000\text{ cm}^{-1}$  with the trapped geometry; this can be due to the pressure the ion pair puts on the molecule restricting the movement of the C-H groups. This group just below  $3000\text{ cm}^{-1}$  is the brightest area in this spectrum and corresponds with the C-H groups stretching, more specifically, the C-H's that point toward fluorine.

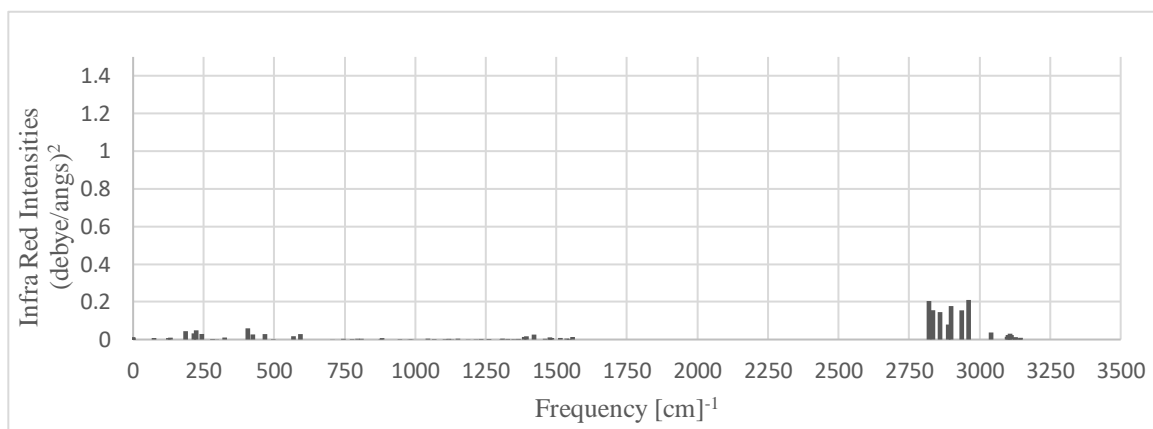


**Figure 2.4.40.** Infrared Spectra of Li-Cyclooctane-F.

The calculated IR spectrum from the side attached Li-F: Cyclooctane (Figure 2.4.41) has unique characteristics that allow detection and differentiation from other systems and isolated molecules. Its brightest peak is  $870\text{ cm}^{-1}$ , the only intense peak in this range for any of the systems. The next most intense peak is located at  $2950\text{ cm}^{-1}$  and is an order of magnitude larger than any of the peaks in this area for the complex Li-Cyclooctane-F. This peak is close in intensity to and blue-shifted from isolated Cyclooctane. Li-F:Cyclooctane contains a band of peaks above  $3000\text{ cm}^{-1}$  similar to that of isolated Cyclooctane, which is due to C-H stretches and is not shifted much, which indicates that Li-F does not strongly interact with the molecule's radial C-H stretches.

The difference between all three spectra can be seen from the overlay in (Figure 2.4.42 and Figure 2.4.43), with Black being isolated Cyclooctane, Blue being from the complex Li-Cyclooctane-F, and Red being from side-attached Li-F:Cyclooctane. Here, we can see the similarities between isolated cyclooctane and the side-attached Li-F:Cyclooctane in the area above  $3000\text{ cm}^{-1}$ . This overlayed spectrum also clearly shows the blue-shift of the brightest peaks in the side attached Li-F:Cyclooctane compared to isolated Cyclooctane, the peak at  $3100\text{ cm}^{-1}$  in Black and  $2950\text{ cm}^{-1}$  Red (Figure 2.4.43).

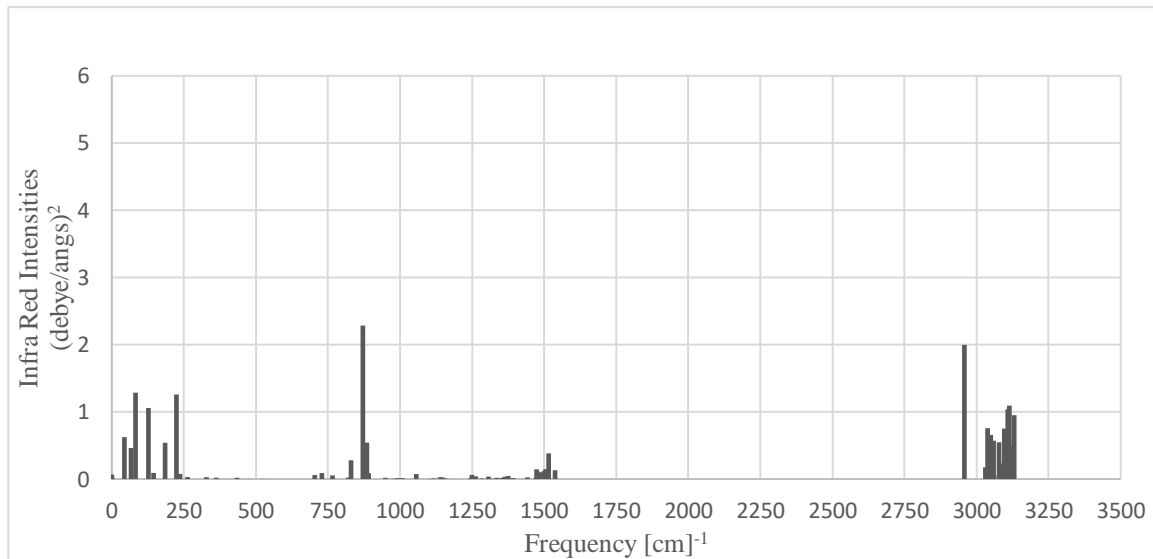


**Figure 2.4.41.** Infrared Spectra of Li-F-Cyclooctane. Side attached.

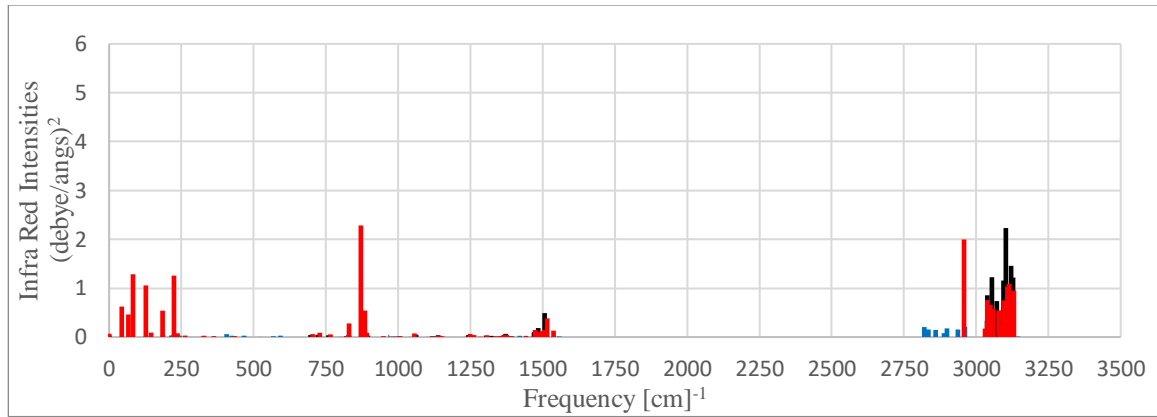


**Figure 2.4.42.** Infrared Spectra Comparison (*Cyclooctane Black, Li-Cyclooctane-F Blue, Li-F-Cyclooctane Red*).

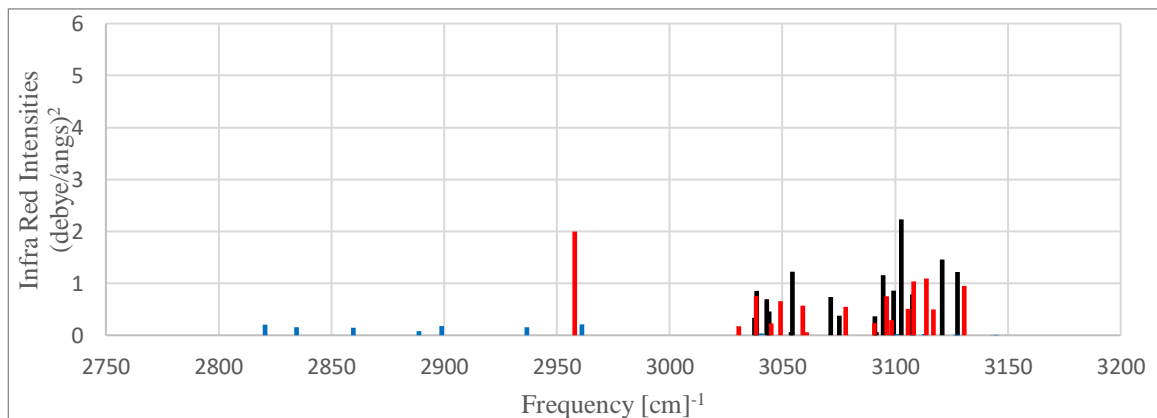


**Figure 2.4.43.** Infrared Spectra Comparison (*Cyclooctane Black, Li-Cyclooctane-F Blue, Li-F-Cyclooctane Red*). Range 2750 cm<sup>-1</sup>- 3200 cm<sup>-1</sup>.

#### 2.4.4 Charges

The calculated charge distribution indicates near-full electron transfer from lithium (except for flipped F-Tetraoxane-Li), and the charge concentration is mainly located on fluorine for all systems. Charge transfers for ion pair complexes are tabulated in (*Table 2.4*). This near-complete electron transfer is consistent for side attached and fluorine pointing systems; however, when lithium points towards Pentaoxecane, the molecule donates a portion of its charge 0.174e to fluorine.

The polar complexes of M-C<sub>6</sub>H<sub>6</sub>F<sub>6</sub>-X have a charge of -0.2 e in the molecule; nonpolar M-C<sub>6</sub>H<sub>12</sub>-X has a charge of -0.15 e residing in the molecule <sup>16</sup>. For Cs-C<sub>6</sub>H<sub>6</sub>F<sub>6</sub>-Cl, Cs/Cl have charges of (+0.84/-0.8) <sup>16</sup> respectively, and Cs-Cl-C<sub>6</sub>H<sub>6</sub>F<sub>6</sub> side-attached Cs/Cl has a charge of (+0.91/-0.94) <sup>16</sup>, indicating that in side-attached where M-X bond is reduced charge transfer is larger. C<sub>3</sub>H<sub>3</sub>F<sub>3</sub> and C<sub>4</sub>H<sub>4</sub>F<sub>4</sub> <sup>15, 19</sup> show similar charge transfers. This is a trend of having lower charge transfer in complexation than inside attached systems; when an ion pair is stretched, the amount of charge transfer from M-X decreases. In Cs-Trioxane-I, the charges are +0.995e for Cs and -0.849e for I <sup>18</sup>, and for Cs-I-Trioxane and Trioxane-I-Cs systems, near complete electron transfers are observed at 0.979e(Cs)/-0.942(I) and +0.928e(Cs)/-0.925e(I) respectively<sup>18</sup>.

Li-Cyclooctane-F has CHELPG ESP chargers on Li/F of +0.775e/-0.847e with a small charge at +0.072e coming from the molecule. Similar charge transfers are seen in the Li-F: Cyclooctane system at +0.735e/-0.812e for Li-F and +0.076e for the molecule. Charge transfers are also primary between M/X in complexes for non-polar analogous systems. Such as in Li-Cubane-f, where Li-cubane-F Li and F carry charges greater than +0.9e and -0.9e, respectively<sup>12</sup>. In M-C<sub>4</sub>H<sub>8</sub>-X, charge transfer for M-X (Li-Cl, Li-I, Cs-Cl) range from (+0.95)-(+1.0) for M, and (-0.91e) – (-0.93e) for X<sup>13</sup>. For Li-C<sub>3</sub>H<sub>6</sub>-F, Li and F have charge transfers of +0.96 and -0.91, respectively <sup>51</sup>. The charge transfer in Li-Cyclooctane-F and side-attached conformers is reduced compared to analogous

systems. This could be explained by the more considerable distance between Li-F in the trapped conformation, but this interpretation does not hold with the Li-F distance in the side-attached system being close to free Li-F's bond length of 1.6 Å. This could be a limitation of the CHELPG ESP method.

The M-C<sub>6</sub>H<sub>6</sub>F<sub>6</sub>-X system was previously studied and found to have a -0.2e charge in the molecule <sup>16</sup>. Similarly, M-C<sub>6</sub>H<sub>12</sub>-X was found to have a charge of -0.15e in the molecule <sup>16</sup>, and this was also the case in M-C<sub>3</sub>H<sub>6</sub>-X and M-C<sub>4</sub>H<sub>8</sub>-X. This differs for cyclooctane complex systems with a slight positive charge of 0.07e. In Cs-C<sub>6</sub>H<sub>6</sub>F<sub>6</sub>-Cl, Cl has a charge of -0.84e, whereas in the Cs-Cl:C<sub>6</sub>H<sub>6</sub>F<sub>6</sub> side-attached Cl has a charge of -0.94e <sup>16</sup>. In Cs- C<sub>6</sub>H<sub>6</sub>F<sub>6</sub>-I complex I has a charge of -0.80e, whereas I has a charge of -0.91e in the Cs- I: C<sub>6</sub>H<sub>6</sub>F<sub>6</sub> side-attached. Therefore, we can see that trapped complexes tend to have lower charge transfer compared to the side-attached for Cs-Cl and Cs-I <sup>16</sup>, this is due to the increased distance between M-X in trapped compared to side-attached conformers.

## Chapter 3. Conclusions

A series of insertion complexes of both polar (tetraoxane and pentaoxecane) and nonpolar (cyclooctane) cyclic molecules in alkali-halide ( $\text{MX}$   $\text{M}=\text{Li}$ ,  $\text{X}=\text{F}$ ) ion-pairs are systematically investigated computationally at the MP2 level of theory. Systems are investigated in terms of structure, stability, polarity, charges, and IR spectra. The investigated trapped molecules, polar and nonpolar, involve several noncovalent interactions such as ion-ion, ion-dipole, ion-induced-dipole, and dipole-dipole interactions.

The high polarity of both polar cyclic molecules (tetraoxane and pentaoxecane) leads to considerable ion affinities to being inserted between the  $\text{Li}-\text{F}$  ion pair. Other conformers include side attached ( $\text{Li}-\text{F}:\text{Mol}$ ) or point ( $\text{F}-\text{Li}-\text{Mol}$ ), where polarity can assist with attachment. This is seen in the considerable  $\text{Li}^+$ -mol attachment energies of 3-6eV, suggesting the reactivity of the system as a  $\text{Li}^+$  acceptor.

The F-Tetraoxane-Li flipped system has exciting properties for energy storage because of its significant negative dissociation energy, with significant energy barriers of around 3eV containing this meta-stable system. Li-Cyclooctane-F also has a sizeable dipole moment; these large polar systems allude to a possible application in light-matter interactions, such as in light detecting/sensing or absorption/utilization.

Formation of the different insertion complexes can be observed by notable concentration and blue-shifting of high-frequency IR spectral lines and by red-shifting lower-frequency IR spectral lines. These changes in the IR intensity spectra are distinguishing features that enable the resolution of attached  $\text{F}-\text{Li}:$   $\text{Mol}$  vs. trapped  $\text{Li}-\text{Mol}-\text{F}$ .

The barrier for the lithium cation to penetrate through all three cyclic molecules to the other side was calculated, which is comparable to the recollection around the cyclic molecules. In the case of Pentaoxecane, the energy barrier for penetration is lower than that for recollecting of the ions around the molecule. Energy barriers for penetrating are significantly lowered when the  $\text{Li}^+$  cation is assisted to the other side by the  $\text{F}^-$  anion; this counter ion provides an attraction force pulling  $\text{Li}^+$  through the molecule. Our findings also show that the energy required to penetrate is reduced with increasing cyclic molecule size; with a larger cyclic molecule, lowered steric forces facilitate an increase in  $\text{Li}^+$ 's ability to penetrate.

The systems could be produced experimentally via photodissociation of the ion-pair  $\text{Li}-\text{F}$  in the presence of Mol (tetraoxane, pentaoxecane, cyclooctane) clusters. This would be followed by the trapping of a Mol by recombining lithium and fluorine. Polar molecules are expected to be trapped more effectively by the two-body stepwise sequence of  $\text{Li}^+ + \text{Mol} \rightarrow \text{Li}^+-\text{Mol}$ , followed by  $\text{Li}^+-\text{Mol} + \text{F}^- \rightarrow \text{Li}-\text{Mol}-\text{F}$ . This would be facilitated by dipole-induced dipole interactions, significantly in the  $\text{Li}^+$ -Tetraoxane and  $\text{Li}^+$ -Pentaoxecane cases with our estimated considerable attachment energies.

When the  $\text{Li}-\text{Mol}-\text{F}$  complexes are formed, they can be identified using IR intensity spectra. These are predicted to be indicators for distinguishing between trapped, attached, pointed, and free Mol in terms of the ratios in the IR intensities that correspond to specific vibrations. This exhibits a possible method for the experimental detection and characterization of polar and non-polar molecules with the attached ion pair such as  $\text{Li}-\text{F}$ .

## **Chapter 4. Future work**

### **4.0 Expansion of work**

The sequential step for this work would be to expand on what is studied here. Starting with trying flipped F-Pentaoxecane-Li to see if it also has interesting properties to the flipped F-Tetraoxane-Li system. Next could be to try increasing the size of the cyclic molecules to 10+ membered groups. Different ion pairs could be tried as well, both alkali metals and halides to compare properties. Penetrating of different ions could be tested, at what size of the cyclic molecule does a larger ion penetrate. Possible changes to the molecules could also be tested, such as replacing oxygens with sulfur or changing the spacing/quantity of polar groups such as C<sub>6</sub>H<sub>12</sub>O<sub>2</sub> (replacing two oxygens in Tetraoxane with two CH<sub>2</sub> groups). Li<sup>+</sup> Penetrating barriers could be more precisely evaluated, this could be done by recalculating geometries (Initial and at the top of the barrier) without the Ne (Fixing atom) present.

### **4.1 Self-assembly**

Given its symmetrical and polar nature, the tetraoxane system could be adapted for self-assembly. One could envision two potential pathways for self-assembly. One is by stacking systems atop one another to create a cylindrical shape. This cylinder could facilitate ion transport. Lithium penetrating in one direction is more favourable (from the Oxygen side towards the Hydrogen side), creating a tiny channel or stream through which lithium ions can flow.

The second possible self-assembly shape is a 2D network, as shown in Figure 4.1.1 This 2D network is composed of tetraoxanes that are rotated by 45 degrees and arranged themselves into a hydrogen-bonded grid. This sheet could act as a membrane favouring the transport of lithium in one direction (hydrogen side to oxygen side).

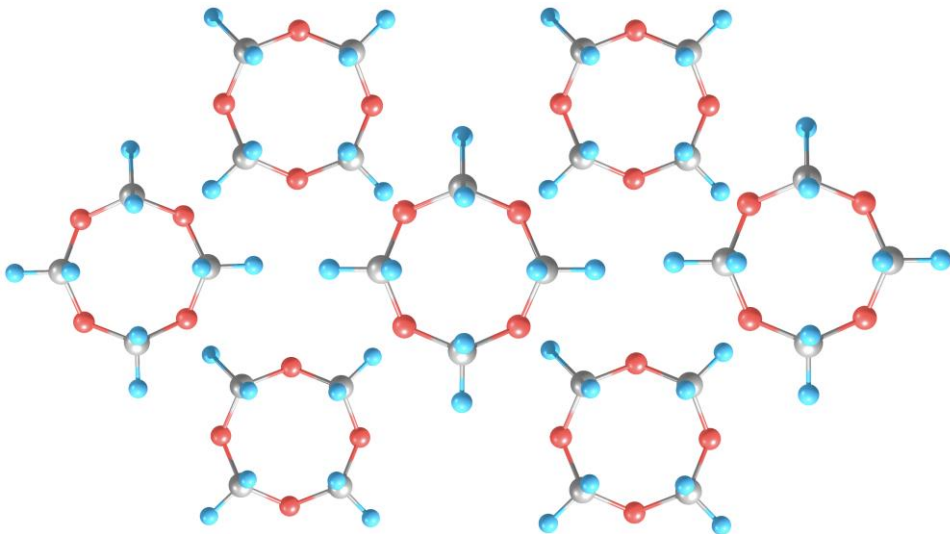


**Figure 4.1.1** 2D Self-Assembled Network of Tetraoxane.

In C<sub>4</sub>H<sub>8</sub><sup>13</sup>, cases of M-X-Mol-M-X were studied; this could also be done with our systems, especially the polar systems. One could envision the expansion of this idea to a growing chain of alternating M-X-Mol-M-X-Mol-M-X... . Each part (Ion-pair or Mol) can help with attachment in the correct orientation of the next building block, as nonpolar systems will not orient opposing ion pairs. In the design of Tetraoxane, each tetraoxane would have the oxygen side pointing towards a Li in Li-F and the Hydrogen side pointing towards the F of Li-F offering stability to this growing chain.

## 4.2 2D network structure

A third potential macro-structure involves bonding tetraoxane to other tetraoxanes, replacing the axial C-H with a C-C bond (Figure 4.2.1). While challenging to create, this carbon-carbon bonded structure would produce a more robust 2D network structure than the hydrogen-bonded network described above. This vital structure would still possess lithium ion penetrating pathways, favouring a direction from hydrogen to oxygen. It could act as a lithium-ion transporter.

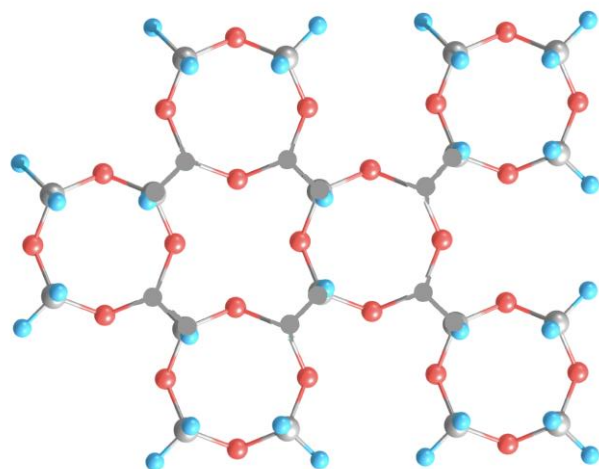


**Figure 4.2.1** 2D C-C bonded network Tetraoxane.

### 4.3 Transmembrane ion-pair transport

Ion-pair receptors are of interest as transmembrane ion transporters<sup>20</sup>. They have the unique ability to recognize and bind to ions. Selectivity is particularly interesting; ion-pair receptors of the correct size (cyclical molecule size) can exhibit enhanced selectivity towards ions of the corresponding size. Small ions like lithium might be better suited to smaller rings and will not bind as tightly as larger ions, such as cesium. It is analogous to a selective membrane/structure permitting a specific ion's passage<sup>52-54</sup>.

In biological systems, the regulated transport of ions across cellular membranes is facilitated by native ion carriers or specialized membrane-embedded proteins. This is a process critical for maintaining optimal physiological functionality. Conversely, abnormal ion transport is directly implemented in various diseases, such as cystic fibrosis. Therefore, developing engineered ion-pair carriers capable of rectifying these transport deficiencies could contribute to therapeutically overcoming these ion-transport-related illnesses.

Lithium is particularly useful in biological applications, having been used to treat the manic episodes of bipolar disorder <sup>55</sup> and for mood stabilization with continued use<sup>56</sup>.

The earliest ion-pair receptors employed for transmembrane ion transport were reported in 2003 <sup>57</sup>. It was found that an organic complex could bind with sodium chloride and potassium chloride to transport the ions across membranes.

## Bibliography

- (1) Eds.; P. J. Linstrom, W. G. M., NIST, Gaithersburg MD. NIST Chemistry WebBook, NIST Standard Ref. Database. <https://webbook.nist.gov/chemistry/>. DOI: <https://webbook.nist.gov/chemistry/>
- (2) Camaioni, N.; Po, R. Pushing the Envelope of the Intrinsic Limitation of Organic Solar Cells. *J Phys Chem Lett* **2013**, *4* (11), 1821-1828. DOI: 10.1021/jz400374p From NLM PubMed-not-MEDLINE.
- (3) Kesters, J.; Govaerts, S.; Pirotte, G.; Drijkoningen, J.; Chevrier, M.; Van den Brande, N.; Liu, X.; Fahlman, M.; Van Mele, B.; Lutsen, L.; et al. High-Permittivity Conjugated Polyelectrolyte Interlayers for High-Performance Bulk Heterojunction Organic Solar Cells. *ACS Appl Mater Interfaces* **2016**, *8* (10), 6309-6314. DOI: 10.1021/acsami.6b00242 From NLM PubMed-not-MEDLINE.
- (4) Wang, P.; Zhu, P.; Wu, W.; Kang, H.; Ye, C. Design of novel nonlinear optical chromophores with multiple substitutions. *Physical Chemistry Chemical Physics* **1999**, *1* (15), 3519-3525, 10.1039/A903535D. DOI: 10.1039/a903535d.
- (5) Katsouras, I.; Asadi, K.; Li, M.; van Driel, T. B.; Kjaer, K. S.; Zhao, D.; Lenz, T.; Gu, Y.; Blom, P. W.; Damjanovic, D.; et al. The negative piezoelectric effect of the ferroelectric polymer poly(vinylidene fluoride). *Nat Mater* **2016**, *15* (1), 78-84. DOI: 10.1038/nmat4423 From NLM PubMed-not-MEDLINE.
- (6) Christopherson, J. C.; Topić, F.; Barrett, C. J.; Friščić, T. Halogen-Bonded Cocrystals as Optical Materials: Next-Generation Control over Light–Matter Interactions. *Crystal Growth & Design* **2018**, *18* (2), 1245-1259. DOI: 10.1021/acs.cgd.7b01445.
- (7) Cavallo, G.; Metrangolo, P.; Milani, R.; Pilati, T.; Priimagi, A.; Resnati, G.; Terraneo, G. The Halogen Bond. *Chem Rev* **2016**, *116* (4), 2478-2601. DOI: 10.1021/acs.chemrev.5b00484 From NLM Medline.
- (8) Clark, T. Halogen bonds and sigma-holes. *Faraday Discuss* **2017**, *203*, 9-27. DOI: 10.1039/c7fd00058h From NLM PubMed-not-MEDLINE.
- (9) Metrangolo, P.; Carcenac, Y.; Lahtinen, M.; Pilati, T.; Rissanen, K.; Vij, A.; Resnati, G. Nonporous organic solids capable of dynamically resolving mixtures of

- diiodoperfluoroalkanes. *Science* **2009**, *323* (5920), 1461-1464. DOI: 10.1126/science.1168679 From NLM PubMed-not-MEDLINE.
- (10) Metrangolo, P.; Neukirch, H.; Pilati, T.; Resnati, G. Halogen bonding based recognition processes: a world parallel to hydrogen bonding. *Acc Chem Res* **2005**, *38* (5), 386-395. DOI: 10.1021/ar0400995 From NLM PubMed-not-MEDLINE.
- (11) Lisac, K.; Topic, F.; Arhangelskis, M.; Cepic, S.; Julien, P. A.; Nickels, C. W.; Morris, A. J.; Friscic, T.; Cincic, D. Halogen-bonded cocrystallization with phosphorus, arsenic and antimony acceptors. *Nat Commun* **2019**, *10* (1), 61. DOI: 10.1038/s41467-018-07957-6 From NLM PubMed-not-MEDLINE.
- (12) Naumkin, F. Y.; Wales, D. J. Counterion-Trapped-Molecules: From High Polarity and Enriched IR Spectra to Induced Isomerization. *Chemphyschem* **2020**, *21* (4), 348-355. DOI: 10.1002/cphc.201901112 From NLM PubMed-not-MEDLINE.
- (13) Cochrane, B.; Naumkin, F. Y. Reshaping and linking of molecules in ion-pair traps. *Chemical Physics Letters* **2016**, *643*, 137-141. DOI: <https://doi.org/10.1016/j.cplett.2015.11.034>.
- (14) Massimo Giamarco, F. Y. N. Carbon-Carbon Bond Formation “Catalyzed” by Ion-Pair Constituents. *ChemistrySelect* **2023**, *8*, e202300057. DOI: <https://doi.org/10.1002/slct.202300057>.
- (15) Naumkin, F. Y. Trapped-molecule charge-transfer complexes with huge dipoles: M-C(2)F(6)-X (M = Na to Cs, X = Cl to I). *Phys Chem Chem Phys* **2008**, *10* (46), 6986-6990. DOI: 10.1039/b807614f From NLM PubMed-not-MEDLINE.
- (16) Naumkin, F. Y. Dipoles inside of dipoles: Insertion complexes of polar versus nonpolar molecules in ion pairs. **2017**.
- (17) Sullivan, M.; Naumkin, F. Y. Highly Polar Insertion Complexes with Focused IR Spectra and Internal Field-Inhibited Isomerization. *Chempluschem* **2020**, *85* (11), 2438-2445. DOI: 10.1002/cplu.202000626 From NLM PubMed-not-MEDLINE.
- (18) Sullivan, M.; Naumkin, F. Y. Supramolecular complexes with insertion-enhanced polarity and tuned IR spectra. *International Journal of Quantum Chemistry* **2020**, *121* (6). DOI: 10.1002/qua.26534.

- (19) Kerr, S.; Naumkin, F. Y. Noncovalently bound complexes of polar molecules: dipole-inside-of-dipole vs. dipole–dipole systems. *New Journal of Chemistry* **2017**, *41* (22), 13576-13584. DOI: 10.1039/c7nj02753b.
- (20) He, Q.; Vargas-Zuniga, G. I.; Kim, S. H.; Kim, S. K.; Sessler, J. L. Macrocycles as Ion Pair Receptors. *Chem Rev* **2019**, *119* (17), 9753-9835. DOI: 10.1021/acs.chemrev.8b00734 From NLM PubMed-not-MEDLINE.
- (21) Carmeliet, E. E. INFLUENCE OF LITHIUM IONS ON THE TRANSMEMBRANE POTENTIAL AND CATION CONTENT OF CARDIAC CELLS. *J Gen Physiol* **1964**, *47* (3), 501-530. DOI: 10.1085/jgp.47.3.501 From NLM.
- (22) Kochhar, G.; Naumkin, F. Y. Insertion complexes of an organic molecule trapped in ion-pairs. *New Journal of Chemistry* **2010**, *34* (12), 2932-2936, 10.1039/C0NJ00510J. DOI: 10.1039/C0NJ00510J.
- (23) Naumkin, F. Y. Dipoles Inside of Dipoles: Insertion Complexes of Polar versus Nonpolar Molecules in Ion Pairs. *J Phys Chem A* **2017**, *121* (23), 4545-4551. DOI: 10.1021/acs.jpca.7b02576 From NLM.
- (24) Trujillo, C.; Sanchez-Sanz, G.; Alkorta, I.; Elguero, J. Simultaneous interactions of anions and cations with cyclohexane and adamantane: aliphatic cyclic hydrocarbons as charge insulators. *J Phys Chem A* **2011**, *115* (45), 13124-13132. DOI: 10.1021/jp205300c From NLM Medline.
- (25) Ziegler, B. E.; Lecours, M.; Marta, R. A.; Featherstone, J.; Fillion, E.; Hopkins, W. S.; Steinmetz, V.; Keddie, N. S.; O'Hagan, D.; McMahon, T. B. Janus Face Aspect of All-cis 1,2,3,4,5,6-Hexafluorocyclohexane Dictates Remarkable Anion and Cation Interactions In the Gas Phase. *J Am Chem Soc* **2016**, *138* (24), 7460-7463. DOI: 10.1021/jacs.6b02856 From NLM PubMed-not-MEDLINE.
- (26) Keddie, N. S.; Slawin, A. M.; Lebl, T.; Philp, D.; O'Hagan, D. All-cis 1,2,3,4,5,6-hexafluorocyclohexane is a facially polarized cyclohexane. *Nat Chem* **2015**, *7* (6), 483-488. DOI: 10.1038/nchem.2232 From NLM PubMed-not-MEDLINE.
- (27) Wudarczyk, J.; Papamokos, G.; Margaritis, V.; Schollmeyer, D.; Hinkel, F.; Baumgarten, M.; Floudas, G.; Müllen, K. Hexasubstituted Benzenes with Ultrastrong Dipole Moments. *Angew Chem Int Ed Engl* **2016**, *55* (9), 3220-3223. DOI: 10.1002/anie.201508249 From NLM.

- (28) Heisenberg, W. A quantum-theoretical reinterpretation of kinematic and mechanical relations. *European Physical Journal A* **1925**, *33* (1), 879-893. DOI: 10.1007/bf01328377.
- (29) Schrödinger, E. Quantisierung als Eigenwertproblem. *Annalen der Physik* **1926**, *384* (4), 361-376. DOI: 10.1002/andp.19263840404.
- (30) Hückel, E. Quantentheoretische Beiträge zum Benzolproblem. *Zeitschrift für Physik* **1931**, *70* (3), 204-286. DOI: 10.1007/BF01339530.
- (31) Jensen, F. Introduction to Computational Chemistry **2017**.
- (32) Griffiths, D. J. *Introduction to Quantum Mechanics*. Cambridge University Press.; 2017.
- (33) Sakurai, J. J., & Napolitano, J. J. . Modern Quantum Mechanics. . Cambridge University Press. **2017**. DOI: <https://doi.org/10.1017/9781108499996>.
- (34) Cramer, C. J. Essentials of Computational Chemistry Theories and Models . **2004**, *Second Edition*.
- (35) Schneider, G.; Fechner, U. Computer-based de novo design of drug-like molecules. *Nat Rev Drug Discov* **2005**, *4* (8), 649-663. DOI: 10.1038/nrd1799 From NLM Medline.
- (36) Ahmad, M.; Dwivedy, A.; Mariadasse, R.; Tiwari, S.; Kar, D.; Jeyakanthan, J.; Biswal, B. K. Prediction of Small Molecule Inhibitors Targeting the Severe Acute Respiratory Syndrome Coronavirus-2 RNA-dependent RNA Polymerase. *ACS Omega* **2020**, *5* (29), 18356-18366. DOI: 10.1021/acsomega.0c02096 From NLM PubMed-not-MEDLINE.
- (37) Gartner, T. E.; Jayaraman, A. Modeling and Simulations of Polymers: A Roadmap. *Macromolecules* **2019**, *52* (3), 755-786. DOI: 10.1021/acs.macromol.8b01836.
- (38) Agarwal, G.; Doan, H. A.; Robertson, L. A.; Zhang, L.; Assary, R. S. Discovery of Energy Storage Molecular Materials Using Quantum Chemistry-Guided Multiobjective Bayesian Optimization. *Chemistry of Materials* **2021**, *33* (20), 8133-8144. DOI: 10.1021/acs.chemmater.1c02040.
- (39) Born, M.; Oppenheimer, R. Zur Quantentheorie der Moleküle. *Annalen der Physik* **1927**, *389* (20), 457-484. DOI: 10.1002/andp.19273892002.
- (40) Cramer, C. J. *Essentials of Computational Chemistry: Theories and Models*; 2002.

- (41) Szabo, A. O., N. S. *Modern Quantum Chemistry: Introduction to Advanced Electronic Structure Theory*; 1996.
- (42) Møller, C.; Plesset, M. S. Note on an Approximation Treatment for Many-Electron Systems. *Physical Review* **1934**, *46* (7), 618-622. DOI: 10.1103/PhysRev.46.618.
- (43) Head-Gordon, M.; Pople, J. A.; Frisch, M. J. MP2 energy evaluation by direct methods. *Chemical Physics Letters* **1988**, *153* (6), 503-506. DOI: [https://doi.org/10.1016/0009-2614\(88\)85250-3](https://doi.org/10.1016/0009-2614(88)85250-3).
- (44) Pople, J. A.; Head-Gordon, M.; Fox, D. J.; Raghavachari, K.; Curtiss, L. A. Gaussian-1 theory: A general procedure for prediction of molecular energies. *The Journal of Chemical Physics* **1989**, *90* (10), 5622-5629. DOI: 10.1063/1.456415.
- (45) Bartlett, R. J. Coupled-cluster theory and its equation-of-motion extensions. *WIREs Computational Molecular Science* **2011**, *2* (1), 126-138. DOI: 10.1002/wcms.76.
- (46) Dirac, P. A. M. A new notation for quantum mechanics. *Mathematical Proceedings of the Cambridge Philosophical Society* **2008**, *35* (3), 416-418. DOI: 10.1017/s0305004100021162.
- (47) Feller, D. The role of databases in support of computational chemistry calculations. *Journal of Computational Chemistry* **1996**, *17* (13), 1571-1586. DOI: 10.1002/(sici)1096-987x(199610)17:13<1571::Aid-jcc9>3.0.co;2-p.
- (48) Valiev, M.; Bylaska, E. J.; Govind, N.; Kowalski, K.; Straatsma, T. P.; Van Dam, H. J. J.; Wang, D.; Nieplocha, J.; Apra, E.; Windus, T. L.; et al. NWChem: A comprehensive and scalable open-source solution for large scale molecular simulations. *Computer Physics Communications* **2010**, *181* (9), 1477-1489. DOI: 10.1016/j.cpc.2010.04.018.
- (49) Breneman, C. M.; Wiberg, K. B. Determining atom-centered monopoles from molecular electrostatic potentials. The need for high sampling density in formamide conformational analysis. *Journal of Computational Chemistry* **2004**, *11* (3), 361-373. DOI: 10.1002/jcc.540110311.
- (50) Wallace, W. E.; Linstrom, P. J.; Mallard, W. G. *NIST Chemistry WebBook*, NIST Standard Reference Database Number 69; 2020.
- (51) Kochhar, G.; Naumkin, F. Y. Insertion complexes of an organic molecule trapped in ion-pairs. *New Journal of Chemistry* **2010**, *34* (12). DOI: 10.1039/c0nj00510j.

- (52) Fu, L.; Yang, Z.; Wang, Y.; Li, R.; Zhai, J. Construction of Metal-Organic Frameworks (MOFs)–Based Membranes and Their Ion Transport Applications. *Small Science* **2021**, *1* (2), n/a. DOI: 10.1002/smss.202000035.
- (53) Zhekova, H. R.; Ngo, V.; da Silva, M. C.; Salahub, D.; Noskov, S. Selective ion binding and transport by membrane proteins – A computational perspective. *Coordination chemistry reviews* **2017**, *345*, 108-136. DOI: 10.1016/j.ccr.2017.03.019.
- (54) Debnath, M.; Chakraborty, S.; Kumar, Y. P.; Chaudhuri, R.; Jana, B.; Dash, J. Ionophore constructed from non-covalent assembly of a G-quadruplex and liponucleoside transports K<sup>+</sup>-ion across biological membranes. *Nature communications* **2020**, *11* (1), 469-469. DOI: 10.1038/s41467-019-13834-7.
- (55) Volkmann, C.; Bschor, T.; Köhler, S. Lithium Treatment Over the Lifespan in Bipolar Disorders. *Front Psychiatry* **2020**, *11*, 377. DOI: 10.3389/fpsyg.2020.00377 From NLM.
- (56) Malhi, G. S.; Tanious, M.; Das, P.; Coulston, C. M.; Berk, M. Potential mechanisms of action of lithium in bipolar disorder. Current understanding. *CNS Drugs* **2013**, *27* (2), 135-153. DOI: 10.1007/s40263-013-0039-0 From NLM.
- (57) Koulov, A. V.; Mahoney, J. M.; Smith, B. D. Facilitated transport of sodium or potassium chloride across vesicle membranes using a ditopic salt-binding macrobicycle. *Org Biomol Chem* **2003**, *1* (1), 27-29. DOI: 10.1039/b208873h From NLM Medline.